

AU-A106 773

HUGHES RESEARCH LABS MALIBU CA

F/G 20/6

REAL-TIME IMPLEMENTATION OF NONLINEAR PROCESSING FUNCTIONS. (U)

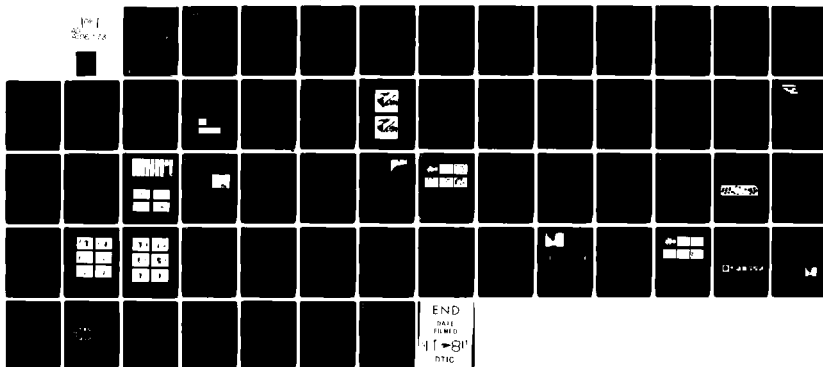
AUG 81 B H SOFFER

F49620-77-C-0080

UNCLASSIFIED

AFOSR-TR-81-0710

NL



LEVEL

4

AD A106773

# REAL-TIME IMPLEMENTATION OF NONLINEAR PROCESSING FUNCTIONS

B.H. Soffer

Hughes Research Laboratories  
3011 Malibu Canyon Road  
Malibu, CA 90265

~~September 1980~~

F49620-77-C-0080

Final Technical Report

For period 15 April 1977 through 14 April 1981

Sponsored by

AIR FORCE OFFICE OF SCIENTIFIC RESEARCH  
Building 410  
Bolling AFB, Washington, D.C.

DTIC  
ELECTE  
NOV 6 1981  
H

DTIC FILE COPY

81 11 06 054

Approved for public release;  
distribution unlimited.

UNCLASSIFIED

SECURITY CLASSIFICATION OF THIS PAGE (When Data Entered)

REPORT DOCUMENTATION PAGE		READ INSTRUCTIONS BEFORE COMPLETING FORM	
1. REPORT NUMBER <b>AFOSR-TR-81-0710</b>	2. GOVT ACCESSION NO. <b>AD-A106</b>	3. RECIPIENT'S CATALOG NUMBER <b>773</b>	
4. TITLE (and Subtitle) <b>REAL-TIME IMPLEMENTATION OF NONLINEAR PROCESSING FUNCTIONS.</b>		5. TYPE OF REPORT & PERIOD COVERED <b>Final Technical Report, 15 April 77 - 14 April 81</b>	
6. AUTHOR(s) <b>H. Soffer</b>		7. PERFORMING ORG. REPORT NUMBER	
8. PERFORMING ORGANIZATION NAME AND ADDRESS <b>Hughes Research Laboratories 3011 Malibu Canyon Road Malibu, CA 93065</b>		9. CONTRACT OR GRANT NUMBER(s) <b>F49620-77-C-0080</b>	
10. CONTROLLING OFFICE NAME AND ADDRESS <b>Air Force Office of Scientific Research Building 410 Bolling AFB, Washington, DC</b>		11. PROGRAM ELEMENT, PROJECT, TASK AREA & WORK UNIT NUMBERS <b>61102F 152305/B1</b>	
12. MONITORING AGENCY NAME & ADDRESS (if different from Controlling Office)		13. REPORT DATE <b>10 August 1981</b>	
		14. NUMBER OF PAGES <b>65</b>	
		15. SECURITY CLASS. (of this report) <b>UNCLASSIFIED</b>	
16. DISTRIBUTION STATEMENT (of this Report)  <b>Approved for public release; distribution unlimited.</b>		17. SECURITY CLASS. (of this abstract)	
17. DISTRIBUTION STATEMENT (of the abstract entered in Block 20, if different from Report)		18. DECLASSIFICATION DOWNGRADING SCHEDULE	
18. SUPPLEMENTARY NOTES			
19. KEY WORDS (Continue on reverse side if necessary and identify by block number)  Optical data processing      Optical digital computing Optical signal processing      Optical analog processing Optical image processing			
20. ABSTRACT (Continue on reverse side if necessary and identify by block number)  Optical data processing has not achieved its potential of increased capacity and speed compared with conventional electronic techniques primarily for lack of a practical real-time image modulator and because optical techniques have been almost exclusively limited to linear operations. The research outlined in this report of a four year research program attacks these issues by studying the implementation of real-time nonlinear parallel-processing techniques. The various			

DD FORM 1 JAN 73 1473 EDITION OF 1 NOV 65 IS OBSOLETE

UNCLASSIFIED

SECURITY CLASSIFICATION OF THIS PAGE (When Data Entered)

UNCLASSIFIED

SECURITY CLASSIFICATION OF THIS PAGE (When Data Entered)

implementations studied all employ real-time liquid-crystal light valves. These spatial light modulators were developed and specially modified for these tasks by Hughes Research Laboratories. One approach we have investigated was to modify and characterize the standard twisted-nematic liquid-crystal devices and then to use them in a coherent optical data-processing apparatus using halftone masks custom designed at the University of Southern California. With the halftone mask technique, we have demonstrated logarithmic nonlinear transformation, allowing us to separate multiplicative images and perform homomorphic filtering. In addition, a novel analog-to-digital converter, based on a modified pure-birefringence liquid-crystal light valve, was developed and demonstrated. It can perform parallel processing using incoherent light, and it promises high data throughput rates. Furthermore, a novel device that converts local light variations to local liquid-crystal phase grating period variations has been fabricated and was evaluated and improved. This device allowed nonlinear functions to be implemented directly without the need for specially made halftone masks. Besides nonlinear analog functions, this device has the demonstrated capability of performing digital optical logic using the binary combinatory Boolean functions. Much materials work remains to be done to produce stable, uniform devices. The project was a cooperative joint effort with the University of Southern California Image Processing Institute.

UNCLASSIFIED

SECURITY CLASSIFICATION OF THIS PAGE (When Data Entered)

# TABLE OF CONTENTS

SECTION		PAGE
1	INTRODUCTION AND BACKGROUND . . . . .	5
2	PROGRESS . . . . .	9
	A. Halftone Screen Processing . . . . .	9
	B. Nonlinear Processing with LCLV Nonlinearities . . . . .	19
	C. Variable Grating Mode Liquid Crystal Device . . . . .	28
	1. Device Physics and Chemistry . . . . .	28
	2. Applications . . . . .	42
3	PERSONNEL . . . . .	59
4	REFERENCES . . . . .	61
5	PUBLICATIONS AND PRESENTATIONS RESULTING FROM AFOSR SUPPORT . . . . .	63
	A. Publications . . . . .	63
	B. Oral Presentations . . . . .	64

AIR FORCE OFFICE OF SCIENTIFIC RESEARCH (AFOSR)  
 NOTICE OF TRANSMITTAL TO DTIC  
 This technical report has been reviewed and is  
 approved for public release in accordance with AFOSR 199-12.  
 Distribution is unlimited.  
 MATTHEW J. KUTNER  
 Chief, Technical Information Division

Accession For		<input checked="" type="checkbox"/>
DTIS GRA&I		<input type="checkbox"/>
DTIC TAB		<input type="checkbox"/>
Unannounced		<input type="checkbox"/>
Justification		<input type="checkbox"/>
By _____		
Distribution/		
Availability		
Dist	Avail	Spec
A		

## SECTION 1

### INTRODUCTION AND BACKGROUND

This final report presents progress made during a four-year program on nonlinear real time optical signal processing. The work includes both the refinement and redesign of already existing liquid crystal light valve (LCLV) optical input transducer types and the development of new species of optical transducers or spatial light modulators. These transducers have been employed in this research effort to produce a variety of demonstrations of nonlinear parallel optical signal processing including applications to digital optical logical computations. This section describes the background and motivation for the research project. The research was done in close cooperation with the Image Processing Institute at the University of Southern California in conjunction with their closely related AFOSR program.

Optical data processing (ODP) has promised for two decades a vast increase in processing capacity and speed, as compared with conventional electronic techniques. This promise has never been fulfilled for several reasons, most notably because of the lack of a practical real-time spatial light modulator, or light valve, and because optical techniques were almost exclusively limited to linear operations. These restrictions recently have been removed by the development of the liquid-crystal light valve by Hughes Research Laboratories (HRL) and the development of certain nonlinear parallel-processing techniques utilizing halftone screens by the University of Southern California (USC) Image Processing Institute. Thus, it was important to determine how successfully nonlinear parallel-processing techniques could be implemented in real time with LCLVs.

The implementation and evaluation of these techniques have a direct relationship to current Air Force technology. Pertinent Air Force interests include multidimensional real-time signal and image processing with varied applications including nonlinear filtering for trajectory control and guidance, "smart" sensing, picture processing, and bandwidth compression. These technologies could benefit substantially from the increased processing capacity and speed that this research may ultimately yield.

Until now, specified nonlinear operations have been performed only with great difficulty. Coherent Fourier optical techniques are essentially restricted to linear operations such as correlation, convolution, and filtering. Electronic digital processing to produce nonlinear transformations is possible, but only in a slow, serial fashion. Certain nonlinearities can be produced by special photographic techniques; but the speed, accuracy, reproducibility, and dynamic range of these techniques are limited.

We have pursued three different optical approaches to attempt to overcome these shortcomings. The first makes use of special halftone screens to modulate the input image, in conjunction with coherent optical processing to desample in the Fourier plane. This technique has made it possible to implement nonlinear functions when selected orders of the halftone diffraction patterns are examined by spatial filtering. Sawchuk and Dashiell of USC have shown, by using specially fabricated halftone screens, how a very wide class of two-dimensional point nonlinear functions can be implemented with a large dynamic range as a function of screen design and diffraction order. The nonlinearities can be continuous or discontinuous. Operations such as taking logarithms, exponentiation, level slicing, intensity bandstopping, and histogram equalization can be performed. We have expanded the halftone screen technique by substituting a real-time photo-modulated LCLV for the static photograph recording medium. We have successfully demonstrated a logarithmic nonlinear transformation using this technique, indicating that this transformation is useful for homomorphic filtering applications. In cooperation with USC, we have studied the performance potentials and limitations of this implementation and how to iteratively modify and improve the LCLV and halftone masks. Limitations due to device hysteresis, poor threshold sharpness, temperature sensitivity, and nonuniformity, though manageable, caused us to seek alternative methods to the halftone screen technique.

The second method studied for overcoming the limitations of serial or photographic nonlinear processing employs an LC effect that can, when incorporated into a new type of light valve, automatically map local image intensity variations into positions in Fourier space. This effect is called the variable grating mode (VGM). Filtering and reconstructing can then yield

many desired nonlinear transformations of the image without the need for specially constructed halftone masks. An additional parameter, the intensity, is made available for processing in this scheme. Using this technique, we have demonstrated the analog operation of level slicing, or isointensity contouring, of a continuous-tone image. Furthermore, recognizing that digital logical operations are merely a special case of nonlinear operations, we have demonstrated a unique, highly advantageous optical computing scheme using this technique. The VGM device itself is still in an early stage of development, and much effort is still needed to develop it into a practical, reliable optical spatial light modulator.

The third method investigated to achieve nonlinear transformations also utilizes an LCLV. In this approach, a pure birefringence light valve and incoherent light are used to produce a unique analog-to-digital (A/D) converter with high throughput. This is a special case of the general technique we investigated to exploit certain inherent nonlinearities of LCLVs.

The work performed in this period, in cooperation with the USC group, has resulted in several technical publications. In this report, we include these papers at selected intervals in the text to provide additional technical detail for the interested reader, rather than repeating the material in appendices. The work is presented topically according to the three broad approaches outlined above.

## SECTION 2

### PROGRESS

#### A. HALFTONE SCREEN PROCESSING

This method of generating nonlinear functions replaces the photographic film, previously employed by Dashiell and Sawchuk at USC, with a standard Hughes liquid crystal light valve operating in the Hybrid Field Effect Mode in order to achieve real-time operation.

In this section we first describe the structure, operating principles, and some operating characteristics of the standard liquid crystal light valve (LCLV). The structure of the present photoactivated LCLV is shown schematically in Figure 1. It includes a sputter deposited CdS photoconductor, a CdTe semiconductor light blocking layer, a multilayer dielectric mirror, and a field-effect liquid crystal layer. All of these are between indium-tin oxide transparent electrodes that have been deposited on glass substrates. A low-voltage (6 to 10 V<sub>rms</sub>) ac drive voltage is impressed across the electrodes. Thin-films of quartz (SiO<sub>2</sub>) are deposited on either side of the liquid crystal layer to protect the liquid crystal from electrochemical degradation.

The device operating principle is straightforward. The thin-film structure is designed to accept most of the drive voltage when the photoconductor is not illuminated; the portion of the voltage that falls across the liquid crystal is below the activation threshold of the liquid crystal electro-optic effect. When light falls on the photoconductor, the photoconductor's impedance drops, thereby switching the voltage from the photoconductor onto the liquid crystal and driving the liquid crystal into its activated state. Thus, the photoconductor acts as a light-activated voltage gate. The high lateral impedance of the thin-films causes very little spreading of the light or of its concomitant liquid-crystal electro-optic effect. As a result, the light activation process is a high-resolution process, and the device can accept photographic quality images for transfer to a coherent beam of light.

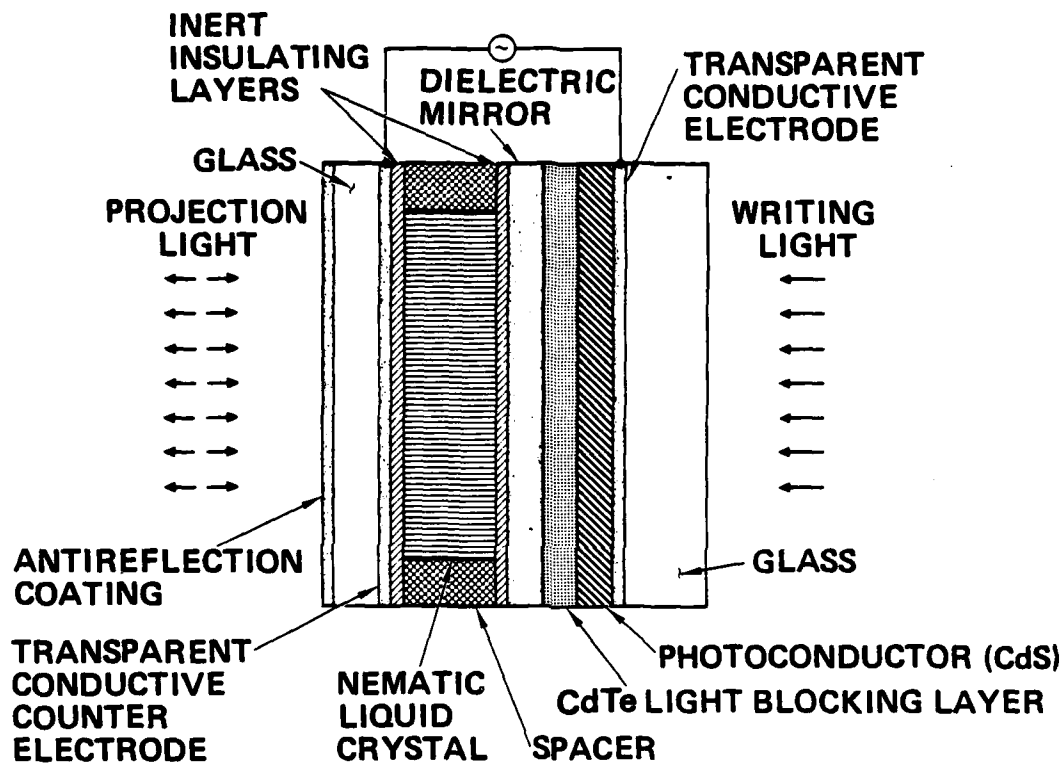


Figure 1. Schematic of the liquid crystal light valve.

### The Hybrid Field-Effect Liquid Crystal Electro-Optic Effect

The biphenyl nematic liquid crystals have positive dielectric anisotropy and are operated in the field-effect mode. The device combines the twisted nematic effect (to create the black off-state) with the optical birefringence effect (to control the transmission of the coherent read-out light in the on-state). Hence, it is called the "hybrid field-effect light valve."

### The Hybrid Field-Effect Mode

The twisted nematic configuration used is not the  $90^\circ$  twist generally used. Because the device operates in the reflection mode, it is impractical to put the polarizer between the dielectric mirror and the liquid crystal. Therefore, the polarizer and the analyzer were both placed on the same side of the liquid-crystal layer. With this arrangement, the  $90^\circ$  twisted nematic effect does not modulate the intensity of the light beam effectively (see below). As a result, we have developed a hybrid field-effect operating mode which uses the  $45^\circ$  twisted nematic effect in the off-state and the pure optical birefringence effect of the liquid crystal in the on-state.

To implement this approach, we fabricated the liquid crystal layer with the liquid crystal molecules at the electrodes aligned with their long axes parallel to the electrode surfaces, but with a  $45^\circ$  angle between the preferred alignment directions on the two electrodes. As a result, molecules across the thickness of the liquid crystal layer rotate through this  $45^\circ$  angle in traversing the space between the electrodes. This twist of the molecular alignment and the intrinsic optical birefringence of the liquid crystal cause the polarization direction of linearly polarized incident light to rotate exactly through the twist angle.

### Operation in the Hybrid Field-Effect Mode

As shown schematically in Figure 2(a), we placed a crossed polarizer/analyzer pair between the light valve and the read-out light source. The polarizer was placed in the incident beam with its polarization direction

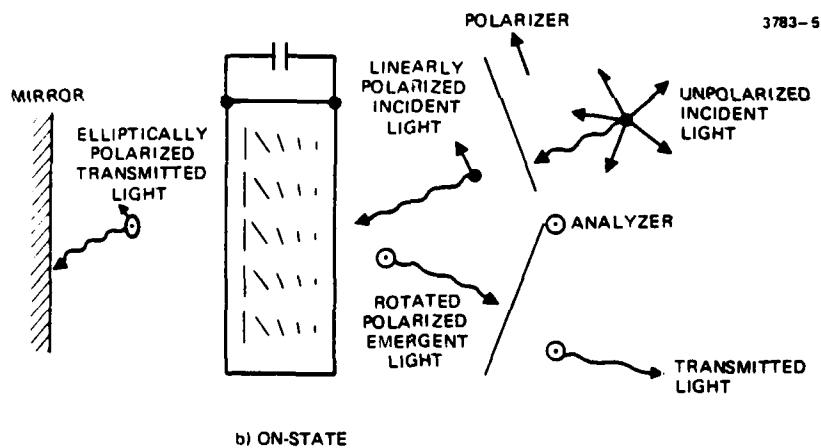
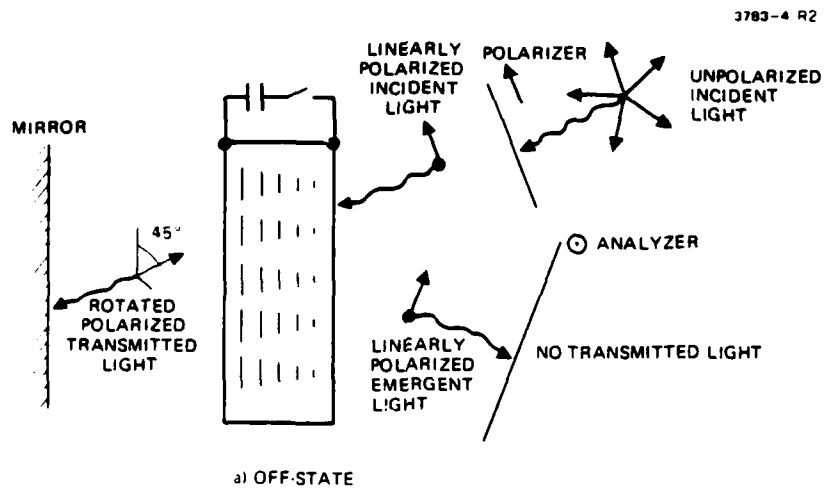


Figure 2. Operating principle of the reflection-mode hybrid-field-effect liquid-crystal device.

oriented so that the polarization direction of the incident light is parallel to the direction of liquid crystal alignment of the entrance electrode. The analyzer was placed in the reflected beam and oriented at  $90^\circ$ , with respect to the polarizer. This provides a dark off-state, since after its first pass through the liquid crystal layer the polarization direction of the linearly polarized incident light is rotated through  $45^\circ$ . But upon reflection from the dielectric mirror, the light passes a second time through the liquid crystal, and its polarization is rotated back to the direction of the incident light where it is blocked by the crossed analyzer. Thus, the off-state of the device is determined entirely by the twisted nematic effect.

If we apply voltage and rotate the molecules completely to the perpendicular alignment (molecules perpendicular to the electrode surfaces), the polarization of the read-out light is unaffected by the liquid crystal and we have a dark on-state as well. But between the off-state and the full on-state there exists a voltage regime where the device will transmit light due purely to the birefringence of the liquid crystal. As voltage is applied to the liquid crystal, the molecules begin to tilt toward the perpendicular alignment (see Figure 2(b)). In this orientation of the molecules (between parallel and perpendicular) the optical birefringence of the molecules will affect the polarization of the light. Since the light that emerges from the device after reflection from the mirror at these intermediate voltages is no longer linearly polarized, transmission occurs. To maximize this transmission, we use a twist angle of  $45^\circ$  rather than the conventional  $90^\circ$  twist. This is done because the effect of the voltage in the on-state of the device on the twisted structure of the liquid crystal is to "snap" (i.e., break) the twist spiral. Half the molecules in the layer adopt the preferred alignment direction associated with one electrode and the other half adopt the alignment direction associated with the other electrode. As a result, the polarization of the light makes an angle of  $45^\circ$  with respect to the molecules in the second half of the cell. This orientation maximizes the net birefringence effect of the light valve. At voltages less than that required to snap the twist of the liquid crystal, the molecules tilt and thereby provide partial transmission. Hence the light valve is capable of continuous tone image conversion.

### Present Performance of the Hybrid Field-Effect Light Valve

The hybrid field-effect light valve, in the present configuration and at its present level of development, has the following basic performance characteristics:

- Aperture size: 1 in.<sup>2</sup>
- Sensitivity (full contrast): 100  $\mu\text{W}/\text{cm}^2$  at 525 nm
- Resolution: 60 lines/mm at 50% MTF
- Contrast: >100:1
- Excitation speed: 10 msec
- Extinction speed: 15 msec
- Reflectivity: >90% (>99% if required)
- Optical quality: <1 wavelength at 6328 Å

To perform nonlinear function transformations a hard clipping, sharp threshold device with a linear, almost vertical transfer characteristic would be ideal. This ideal can be approached to some degree with a thicker CdS photoconductor layer in the LCLV. We have fabricated such a device and have indicated the input/output characteristics of this thick CdS LCLV in Figure 3; in particular, the "on" and "off" states. The 200 Hz curve, which is somewhat steeper than the 2 kHz curve, shows a greater gamma. Most important is the remarkable difference in overall shape of the transfer characteristic. It is known that deviations from linearity and sharp cutoffs at the shoulders and toes will degrade device performance. To what degree and in what fashion have been studied in cooperation with USC by computer simulations. The detailed results may be found in the thesis of Ahmad Armand, USC EE Department, June 1979.

### Logarithmic Transformation and Homomorphic Filtering

With the halftone mask technique where a custom-designed screen is used in conjunction with the LCLV to implement nonlinear functions in real

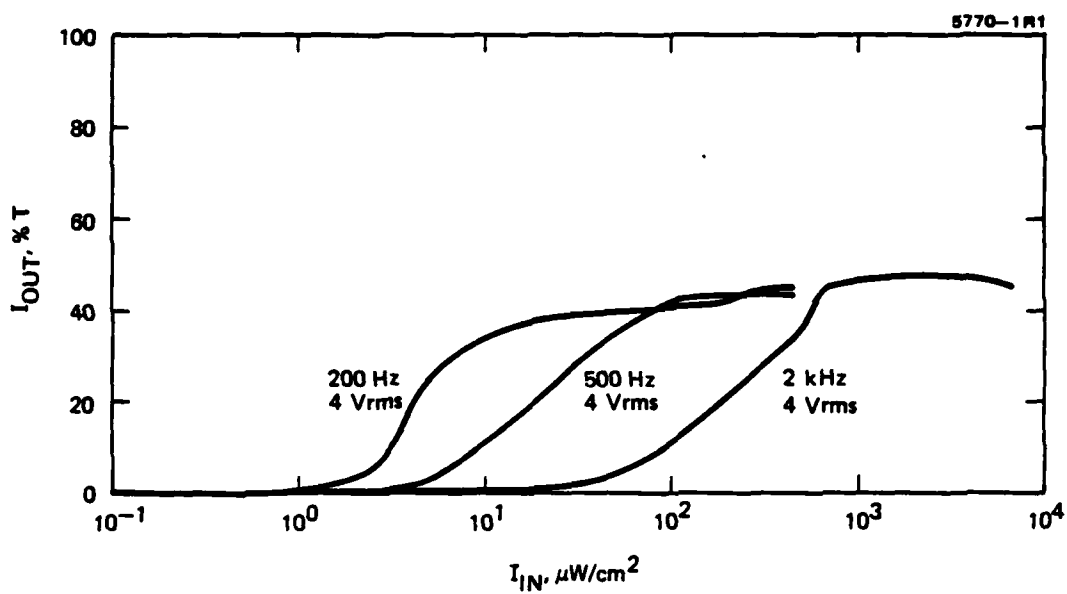


Figure 3. Input/output characteristics of a thick CdS LCLV.

time, the logarithmic function was used to transform multiplicative images into additive ones. These images were then linearly optically filtered.

A half-tone screen designed at USC (see the corresponding report under Grant AFOSR-77-3285) for matching the transfer characteristics of a well-behaved light valve which showed little hysteresis was successfully used to generate the logarithmic function over a dynamic range of two orders of magnitude with an accuracy of  $\pm 10\%$ , or  $1\text{-}1/2$  decades with an accuracy of  $\pm 5\%$ . The original transfer function and the generated logarithmic transfer function are in the semi-logarithmic plots in Figure 4. Experiments were performed to demonstrate a real-time application of the logarithmic transformation by converting a multiplicative image into an additive one. The optical Fourier transform spectrum of two perpendicularly crossed (multiplied), coarse, intensity gratings, tilted at  $45^\circ$  to the horizontal, is shown in the upper portion of Figure 5. This was obtained by imaging the product of the grating transmission on the light valve input in its normal mode of operation. This is the expected diffraction pattern of two crossed gratings; "cross-terms" are visible in the corners of the square in the upper figure. The pattern is not simply the sum of the diffraction patterns of the two gratings. Operating the LCLV with a logarithmic transfer function (by inserting the half-tone mask in series with the LCLV) transforms the multiplicative spectrum into an additive one. The lower portion of Figure 5 shows the result of simply inserting the half-tone screen mask in series with the input imaged on the LCLV (see Figure 6). The photographic exposure is equal in both the upper and lower parts of Figure 5. The 0th, 1st, and 2nd orders indicated are diffraction orders of the fine periodicity half-tone mask. In the 0th order, for which the mask was designed, cross terms are absent from the crossed grating diffraction, which demonstrates the transformation from multiplication to addition.

Further attempts at refining the logarithmic half-tone screen based on the transfer function actually obtained from the first screen did not yield any significant improvement. The operating region was shifted toward the low-intensity knee of the LCLV characteristic curve to lessen the optical power required, but no improvement in dynamic range or linearity was achieved.

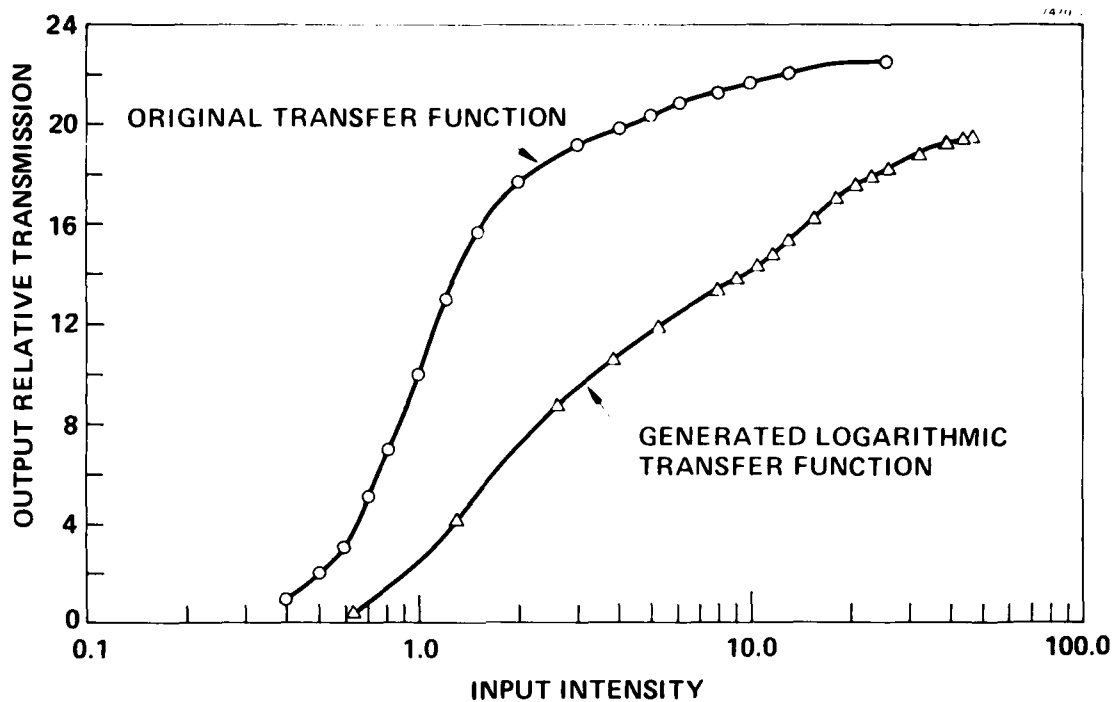


Figure 4. LCLV transfer function and generated logarithmic transfer function.

7470 1

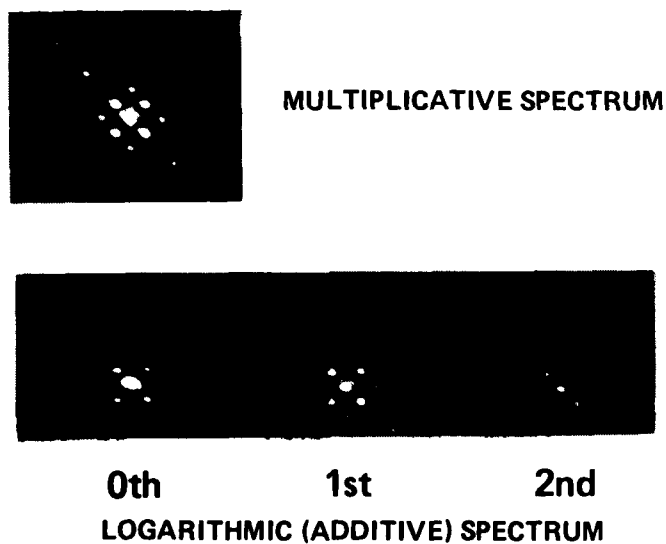


Figure 5. Crossed grating diffraction: multiplicative and additive.

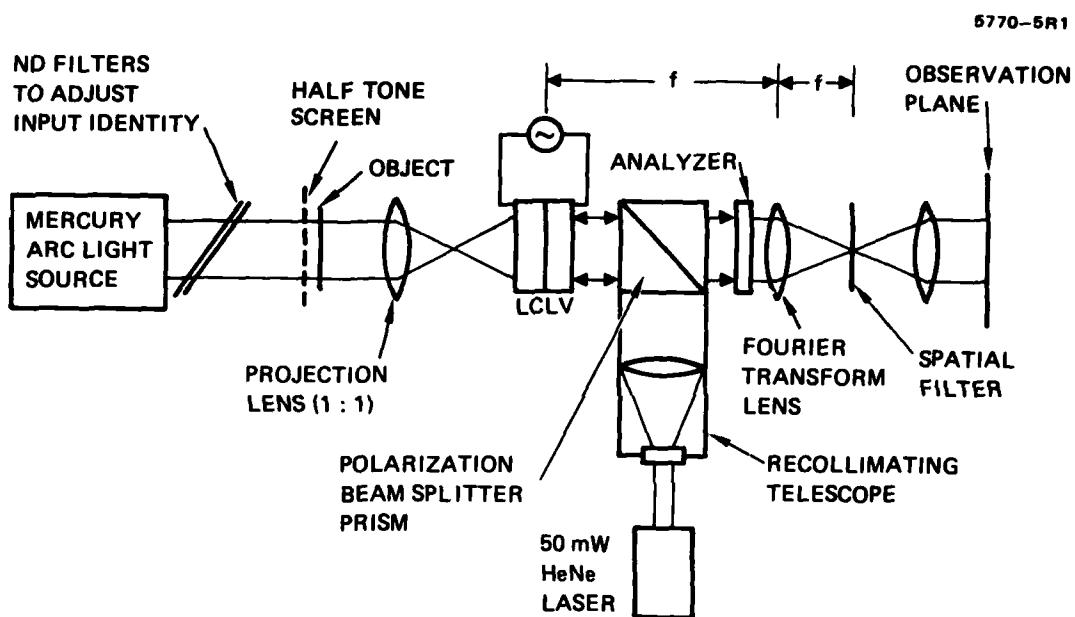


Figure 6. Experimental setup of coherent ODP system.

An experiment was performed that successfully demonstrated the concept of homomorphic filtering. A bar pattern simulating a video raster scanner noise was multiplied with a continuous tone image. This multiplicative noise can be seen as the vertical bars in Figure 7(a). After taking the logarithm, the noise is absent, the Fourier spectrum is greatly simplified, and the cross terms are removed. Now the bar pattern can be easily filtered out by the standard techniques of linear optical filtering in Fourier space. This process is called homomorphic filtering. The resulting filtered image in our example is shown in Figure 7(b).

Many problems surfaced regarding the standard LCLV, which, of course, had originally been developed for use in display applications. In its intended applications, there was a greater tolerance for errors of temperature sensitivity, repeatability, and uniformity of response than can be admitted in ODP applications. Furthermore, for nonanalytic nonlinearities with sharp jumps, a very sharp threshold LCLV transfer function would be needed. These LCLV problems are presently being addressed in separate projects, and until they are resolved, no further halftone screen work with the LCLV is recommended.

#### B. NONLINEAR PROCESSING WITH LCLV NONLINEARITIES

As an example of performing nonlinear real-time optical processing directly with the nonlinearities of LCLVs, we have demonstrated a parallel A/D converter. No halftone screen techniques are needed in this application. The technique depends essentially on the quasi-sinusoidal transfer function of a "pure birefringent" or "tunable birefringence" LCLV. This A/D converter does not need coherent light, and no Fourier processing is done. The number of bits is limited by the aperiodicity of the transfer function, and until special schemes are found to rectify this characteristic, further work is not recommended on this particular application. We present below a reprint of a paper published in Optics Letters with additional technical details, following a brief description of the theory and operating characteristics of this special LCLV employed in the A/D converter.

8903-1



UNFILTERED IMAGE

Figure 7(a). Original object with multiplicative raster scanner noise.

8903-2



FILTERED IMAGE W/HALFTONE SCREEN

Figure 7(b). Image after homomorphic filtering.

### Tunable Birefringent Light Valve Operation

This mode of light valve operation is employed in the parallel A/D converter described later in this section. The intrinsic nonlinearity of the device is used to advantage for data processing.

The large anisotropy of refractive index in nematic liquid crystals can be utilized directly to make a field-effect device. The diagram in Figure 8 illustrates a tunable-birefringence LCLV in which a nematic of negative dielectric anisotropy is aligned with its director essentially perpendicular to the electrode surfaces. In the off-state, plane-polarized incident light travels down the optic axis of the liquid crystal, is reflected back, and is absorbed by a crossed polarizer (analyzer). When a field above a critical threshold voltage (typically 3 to 10 V) is applied, the liquid crystal begins to turn away from the direction of the applied field, and then it no longer appears isotropic to the normal incident light. The liquid crystal film shows a birefringence effect that increases with the applied voltage. This introduces a large phase retardation so that a given wavelength of light passes through the analyzer in a series of maxima and minima as the voltage is increased.

Generally, the transmission of a birefringent ( $\Delta n$ ) layer between cross polarizers is expressed as

$$T = \sin^2 2\phi \sin^2 \frac{\pi d \Delta n \sin^2 \theta}{\lambda} ,$$

where  $\theta$  is the angle between the liquid-crystal optical axis and the incident light,  $\phi$  is the angle between the input polarization and the direction of the tilt of the liquid-crystal optical axis, and  $d$  is the cell thickness. This optical effect that the liquid crystal has on the light beam has been treated as a function of the orientation of the liquid-crystal molecules. However, if the liquid crystal has a positive dielectric anisotropy (the dielectric dipole moment is parallel to the optical axis), a voltage above a certain value will tilt the liquid-crystal molecules. This corresponds to a change in the angle  $\theta$  (in the above case, from  $90^\circ$  to lower values), which

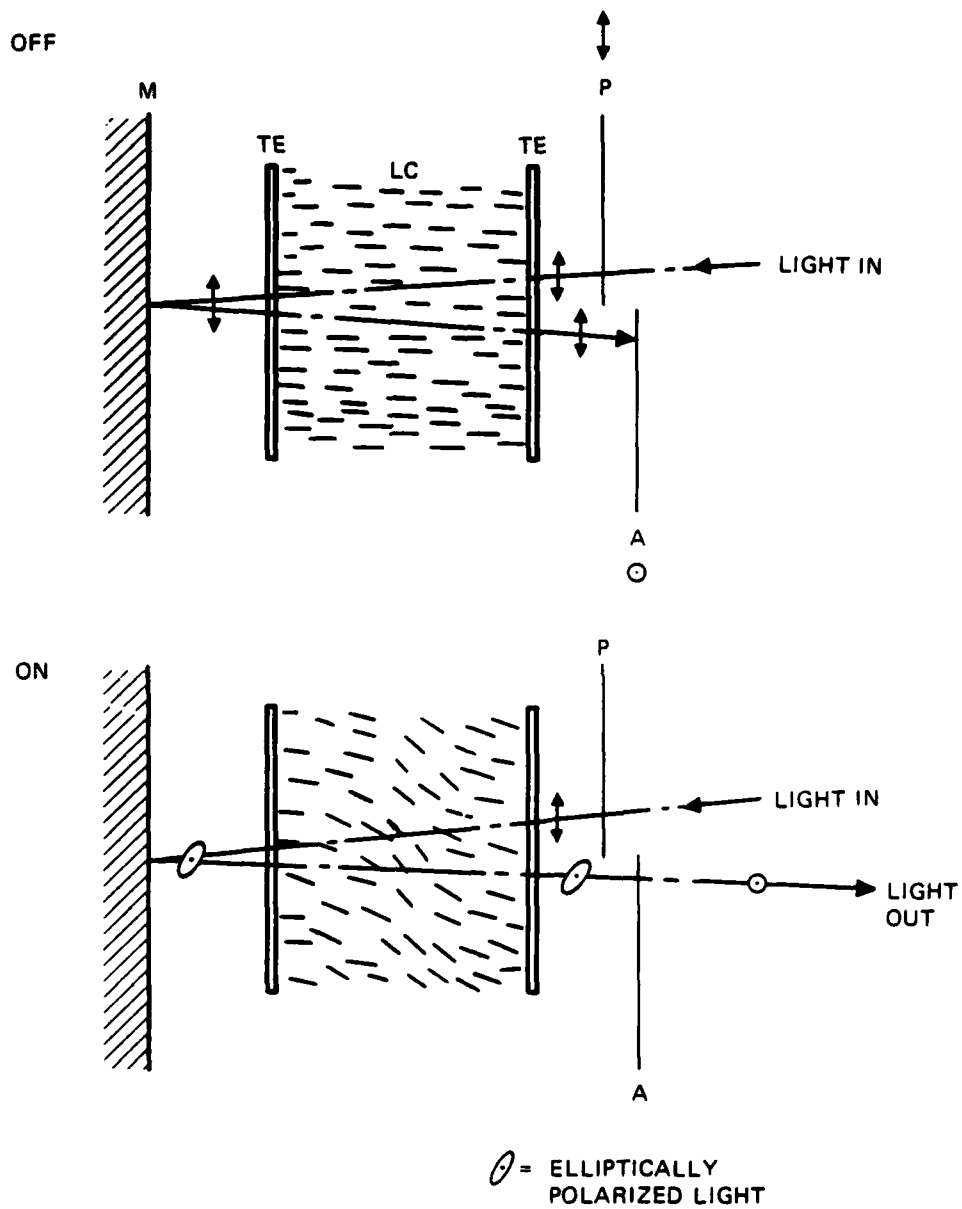


Figure 8. Diagram of a tunable-birefringence field-effect cell (P = polarizer, A = analyzer, TE = transparent electrode, M = mirror, LC = liquid crystal).

means a change in the optical retardation and thus a change in the transmission. In general, the optical transmission is a multiple peaked function of the applied voltage. This is shown in Figure 9 for the transmission of three different wavelengths in a test cell containing a Schiff base nematic mixture of N-(p-methoxybenzylidene)-p-butylaniline. The different colors, although not separated in their first transmission peak above threshold, become better separated at higher voltages. As a result, with incident white light, the viewer sees no light below  $V_{th}$  at first. Then, gray, white, and a sequential series of Newton colors appear as the cell voltage increases. The optimum transmission effects are obtained when the liquid-crystal director is realigned uniformly by the field with its  $\phi$  angle at  $45^\circ$  with respect to the incident polarized light. This can be accomplished by introducing a slight pre-tilt of the liquid crystal in that direction in the off-state. The more monochromatic the light, the better defined the modulation of transmission will be.

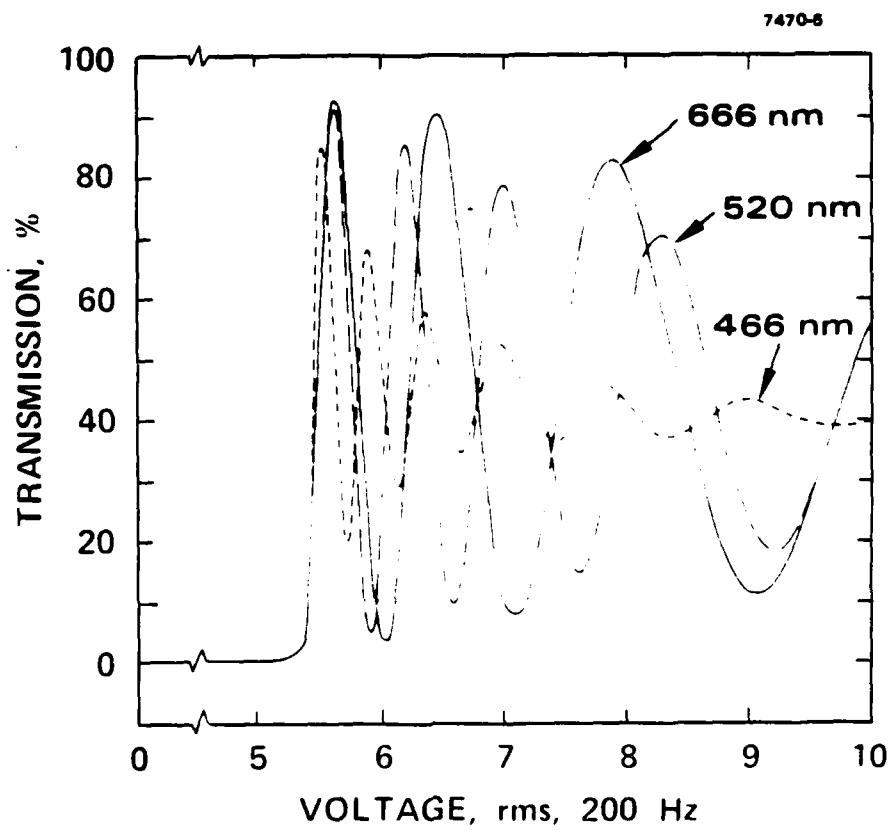


Figure 9. Transmission characteristics of a tunable birefringence cell between crossed polarizers (Schiff-base mixture, surface-perpendicular alignment).

# Real-time parallel optical analog-to-digital conversion

A. Armand, A. A. Sawchuk, and T. C. Strand

Department of Electrical Engineering, Image Processing Institute, University of Southern California, Los Angeles, California 90007

D. Boswell and B. H. Soffer

Hughes Research Laboratories, 3011 Malibu Canyon Road, Malibu, California 90265

Received August 24, 1979; revised manuscript received December 6, 1979

A technique for optically performing parallel analog-to-digital conversion on incoherent two-dimensional inputs at real-time rates is described. The system uses a birefringent optical real-time input transducer combined with a detector array and optical thresholding. Quantization and bit plane outputs are produced in parallel without scanning. An experimental system with three-bit accuracy is described.

The process of analog-to-digital (A/D) conversion is the representation of continuous analog information in sampled and quantized form. For one-dimensional signals, any coding procedure that assigns to each signal value a group of digits (bits) performs such an operation. For digital processing of multidimensional signals and images, the sampling, quantization, and digitization must be performed on an array of data. We describe here a technique of real-time incoherent nonlinear optical processing that performs two-dimensional A/D conversion of images or other page-organized data in parallel without the need for scanning. The method relies on the nonlinear characteristics of real-time optical input devices, such as the Hughes liquid-crystal light valve (LCLV)<sup>1-4</sup> or the Itek Pockels readout optical modulator (PROM).<sup>5</sup>

Optical A/D conversion has been achieved for single-point inputs by electro-optical methods<sup>6</sup> in real time. Other techniques of nonlinear optical processing have performed A/D conversions by halftoning methods, although not in real time.<sup>7-10</sup>

The LCLV, PROM, and many other real-time optical input transducers rely on electro-optically controlled birefringence to produce a spatially varying linear differential phase retardation along two axes of a crystal. For this work a LCLV has been constructed with uniform perpendicular alignment of the liquid-crystal material so the device exhibits a pure birefringent effect that varies with local electric field. When the LCLV is placed between crossed polarizers, a sinusoidal variation of intensity transmittance with applied voltage is observed.<sup>3-5</sup> When a photoconductor is placed at the surface of the liquid-crystal cell, the local electric field is a function of the incident illumination.<sup>1,2</sup> The overall relationship between the intensity transmittance of the device and the incident intensity at any point is given ideally by the sinusoidal curve shown with dashes in Fig. 1(a).

The digital results of A/D conversion at each image point may be output serially as a bit sequence or in parallel as bit planes.<sup>11</sup> Bit planes are binary image planes, each of which displays the information of a

particular significant bit of the digitized image. The solid-line curves of Fig. 1 show the nonlinear transfer characteristic needed to produce the bit planes of the three-bit reflected binary or Gray code and their relationship to the dashed curves of sinusoidal device characteristics. When the output of Fig. 1(a) is thresholded at one half, a 1 output is produced above threshold and a 0 output below, as shown by the curves with solid lines. This thresholding can be done electronically following light detection by a parallel array of sensors. The threshold output in Fig. 1(a) is the least significant bit of the three-bit Gray code. The other two bits are obtained by attenuating the input intensity effectively to rescale the horizontal axis. Use of the full dynamic range (0 to 8) gives the least significant bit. Attenuating the input by a factor of  $1/2$  (to the range 0

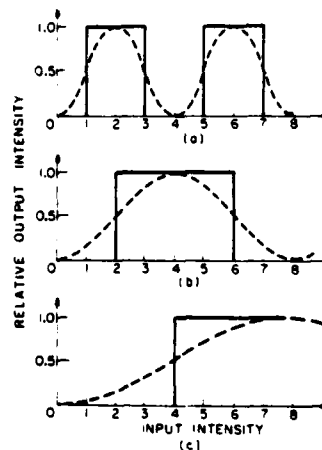


Fig. 1. Nonlinear characteristic curves required for the three-bit Gray code. Solid curves are the desired characteristics for the bit plane outputs. Dotted curves are the ideal sinusoidal responses of a linear birefringent device. Parts (a) through (c) represent increasingly significant output bits.

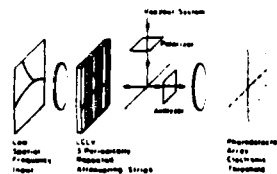


Fig. 2. System for parallel A/D conversion.

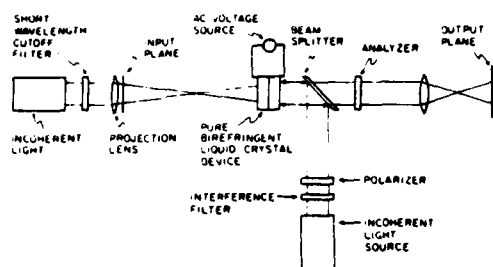


Fig. 3. Experimental setup for real-time parallel analog-to-digital conversion.

to 4) gives the first cycle of the characteristic curve shown in Fig. 1(b). The last (most significant) bit is obtained by using an attenuation of one fourth so the curves of Fig. 1(c) result. Note that any continuous input between 0 and 8 gives a unique quantized three-bit output. Although the thresholded outputs in Fig. 1 are the three bits of the Gray code, other A/D code conversions, such as the usual straight binary code, can be achieved by translating these curves left or right along the horizontal axis. This can be done by introducing phase-retardation plates with different delays along orthogonal axes into the crossed polarizer system.

The system can produce these bits in parallel by placing an array of three periodically repeated attenuating strips over the write surface of the liquid-crystal device, as shown schematically in Fig. 2. The strips have attenuation factors of 1,  $\frac{1}{2}$ , and  $\frac{1}{4}$ , and the image of the strips is in register with a parallel photodetector array with electronic thresholding in the output plane. All three bits are sensed in parallel in this way. The period of the strips should be much smaller than the inverse of the maximum spatial frequency of the input picture to avoid aliasing. A two-dimensional array of attenuating spots with a corresponding detector array can also be used instead of the linear strip array. Simpler but slower operation can be achieved by using only one detector array and sequentially uniformly attenuating the entire input array. Ideas such as this have been used for electro-optic A/D conversion,<sup>6</sup> but none have used an optically controllable real-time device.

The experimental system shown in Fig. 3 was used to obtain the input-output characteristic of the pure birefringent LCLV and to demonstrate the concept. The incoherent source illuminating the input plane is a mercury-arc lamp. A fixed and rotatable polarizer pair in the input-light beam is used to vary the input-light

intensity. The real-time device was a Hughes perpendicularly aligned nematic LCLV with a CdS photoconductor. The short-wavelength cutoff filter eliminates wavelengths shorter than 493 nm to make sure that the write-beam wavelength is matched to the sensitivity range of the CdS photoconductor. The read light source is a xenon-arc lamp. Because of the dispersion of birefringence in the liquid-crystal material, the read light should have a narrow spectral bandwidth. An interference filter with a peak wavelength of 434.7 nm and a bandwidth of 18.4 nm was used to meet this requirement for the read light. With no picture in the input plane, the output intensity varies in a quasi-sinusoidal fashion with increasing input illumination because of the changing birefringence. If the amount of birefringence varied linearly as a function of the write-beam intensity, a strictly sinusoidal variation of the output intensity would be expected. However, a number of factors, including the optical nature of the liquid crystal and the photoconductor characteristic properties, affect the output curve and produce an approximately sinusoidal output whose frequency varies (monotonically) with input intensity. The experimental response curve obtained is shown in Fig. 4.

Although the theory behind the A/D conversion assumes a strictly periodic response characteristic, it is possible to produce the desired bit planes by using the quasi-periodic response curves of the actual device. The trade-off is that nonuniform quantization results. The quantization levels obtained in this experiment are indicated in Fig. 4.

There are no attenuating strips on the liquid-crystal device used in this experiment. Instead, the bit planes were generated serially. Also, the output was recorded on hard-clipping film rather than a thresholding detector array. A test target was generated that consisted of an eight-gray-level step tablet. The gray levels were chosen to match the quantization levels shown in Fig. 4. This test object was imaged onto the liquid-crystal device, and the output was photographically hard clipped to produce the least significant bit plane of a three-bit A/D conversion. Next the write illumination intensity was decreased, effectively rescaling the response curve of the device to generate the next bit plane. The last bit plane (most significant bit) was obtained by attenuating the write intensity again and photographing the output. The input and the three-bit planes generated are shown in Fig. 5.

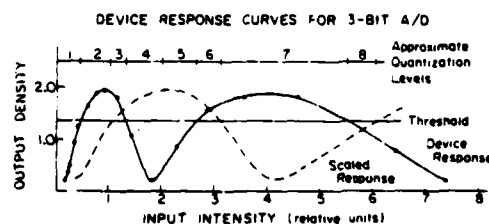


Fig. 4. Response curve of the liquid-crystal device used for the three-bit A/D conversion. The solid curve is the measured response. The dotted curve represents the same response with a fixed attenuation of the input.

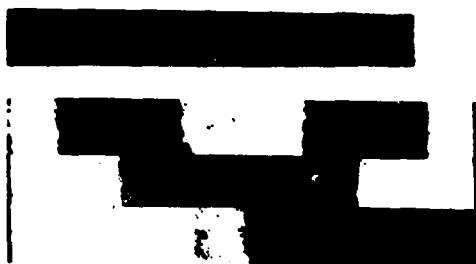


Fig. 5. Direct analog-to-digital conversion. The eight-level analog input is shown at the top. Below is the binary-coded output in the form of three bit planes of the Gray code.

Although the output contains some noise, the experiment illustrates the principle of real-time parallel incoherent optical A/D conversion. It was found later that the computer-generated gray scale was somewhat noisy because of the grain of the high-contrast film used. It is possible that future experiments with cleaner inputs and improved periodic light valves could produce better experimental results and more bits of quantization.

The potential A/D conversion rate can be estimated from typical parameters of currently available devices. The important parameters are device resolution (typically 40 cycles/mm), device size (typically 50 mm  $\times$  50 mm), and speed (generally 30 frames per second). Multiplying all these parameters together and dividing by 3 for the attenuating strips implies an A/D conversion rate of  $4 \times 10^7$  points per second. A fully parallel system with one light valve and detector array for each bit plane could achieve  $1.2 \times 10^8$  points per second.

The feasibility of real-time parallel A/D conversion on two-dimensional inputs has been shown in this experiment. In contrast with other techniques of real-time nonlinear optical processing, such as halftoning,<sup>12-14</sup> the system operates with incoherent input. The requirements on the spatial and temporal coherence of the readout illumination are sufficiently relaxed that noise problems associated with coherent spatial filtering or transforming techniques are avoided. This technique also minimizes the spatial-frequency requirements of the real-time device because the sharp edges of the binary dots in halftoning do not have to be maintained.

Although these initial results are encouraging, further application of the technique must await improved real-time devices. The aperiodic nature of the LCLV results in unequal quantization intervals and limits the number of bits. The LCLV device used in this experiment is inherently aperiodic because of the nonlinear response of the photoconductor and the nonlinear relationship between applied voltage and effective bire-

fringence. By altering the real-time device itself, the response may be improved somewhat. The possibility of making real-time devices (with liquid-crystal or PROM technologies) having a periodic response is being investigated.

This research was supported by the Air Force Office of Scientific Research, Electronics and Solid State Sciences Division, under Grant AFOSR-77-3285 at USC and Contract F49620-77-C-0080 at Hughes Research Laboratories.

This work was presented in part at the Optical Society of America Annual Meeting, October 1978 [J. Opt. Soc. Am. 68, 1361A (1978)].

## References

1. T. D. Beard, W. P. Bleha, and S.-Y. Wong, "AC liquid/crystal light valve," *Appl. Phys. Lett.* **22**, 90 (1974).
2. J. Grinberg *et al.*, "A new real-time non-coherent to coherent light image converter," *Opt. Eng.* **14**, 217 (1975).
3. A. Armand, D. Boswell, A. A. Sawchuk, B. H. Soffer, and T. C. Strand, "Real-time nonlinear optical processing with liquid crystal devices," in *Proceedings of the IEEE 1978 International Optical Computing Conference* (Institute of Electrical and Electronics Engineers, New York, 1978), pp. 153-158.
4. A. Armand, D. Boswell, A. A. Sawchuk, B. H. Soffer, and T. C. Strand, "Approaches to nonlinear optical processing in real-time," in *Proceedings of the International Commission for Optics Congress* (Institute di Optica, Madrid, 1978), pp. 253-256.
5. S. Iwasa and J. Feinleib, "The PROM device in optical processing systems," *Opt. Eng.* **13**, 235 (1974).
6. H. F. Taylor, "An electrooptic analog-to-digital converter," *Proc. IEEE* **16**, 1524 (1975).
7. A. W. Lohmann and T. C. Strand, "Analog-to-digital conversion of pictures with optical means," in *Proceedings of Electro-Optics International Laser Conference* (Industrial and Scientific Conference Management, Inc., Chicago, Ill., 1975), pp. 16-21.
8. T. C. Strand, "Non-monotonic nonlinear image processing using halftone techniques," *Opt. Commun.* **15**, 60 (1975).
9. H. K. Liu, "Coherent optical analog-to-digital conversion using a single halftone photograph," *Appl. Opt.* **17**, 2181 (1978).
10. H. K. Liu, "New and direct optical analog-to-digital conversion method," *Opt. Lett.* **3**, 244 (1978).
11. W. K. Pratt, *Digital Image Processing* (Wiley-Interscience, New York, 1978), Chap. 12.
12. H. Kato and J. W. Goodman, "Nonlinear filtering in coherent optical systems through halftone screen processes," *Appl. Opt.* **14**, 1813 (1975).
13. S. R. Dashiell and A. A. Sawchuk, "Nonlinear optical processing: analysis and synthesis," *Appl. Opt.* **16**, 1009 (1977).
14. J. W. Goodman, "Operations achievable with coherent optical information processing systems," *Proc. IEEE* **65**, 29 (1977).

### C. VARIABLE GRATING MODE LIQUID CRYSTAL DEVICE

During this program, we pursued several tasks which aimed at improving our understanding of the VGM effect and at developing the VGM photoactivated light valve device. In the VGM effect, certain LC materials exhibit a transparent phase grating whose local period is proportional to the locally applied voltage. When incorporated into a light valve sandwich structure, along with a photoconductive layer, local variations in the spatial distribution of the light signal or image intensity are converted into local variations of the grating period. In the Fourier transform plane, a novel additional parameter - the intensity - is coded into the spatial frequency distribution in a way that allows greater freedom to perform nonlinear optical data and image processing and to perform optical computations as well by simple spatial filtering and re-synthesis. We have examined many aspects of the device, including the LC system itself, the photo-conductive and electrical properties of the light valve, a new LC alignment scheme, and the detailed optical polarization properties of the VGM diffraction patterns. Furthermore, we have demonstrated several applications of the VGM device as well, both in analog nonlinear processing and in optical digital computation.

#### 1. Device Physics and Chemistry

This section describes the main results on device physics and chemistry. The published paper "Variable Grating Mode Liquid Crystal Device for Optical Processing" given at the SPIE LA Technical Symposium, February 1980, is included here and contains a concise summary and exposition of the basic properties of the VGM effect and device.

## Variable grating mode liquid crystal device for optical processing

B. H. Soffer, D. Boswell, A. M. Lackner

Hughes Research Laboratories, 3011 Malibu Canyon Road, Malibu, California 90265

A. R. Tanguay, Jr., T. C. Strand, A. A. Sawchuk

University of Southern California, Los Angeles, California 90007

### Abstract

*In the variable grating mode (VGM) operation of a liquid crystal device, a phase grating is formed whose period depends upon the voltage placed across the cell. Typical spatial frequency variation is from 100 to 600 cycles/mm. By adding a photoconductive layer to the cell, the grating period can be optically controlled. Thus each input intensity level in an optical signal will generate a local grating structure at a different spatial frequency. If the VGM device is placed in the input plane of a coherent optical processor, each point in the Fourier transform domain will correspond to a different grating frequency, and thus to a different input signal level. By varying the attenuation at each point in the Fourier plane, any desired transformation of input intensity to output intensity can be achieved. In particular, level slicing can be achieved by placing a slit in the filter plane so that only a narrow range of spatial frequencies is transmitted and thus a narrow range of input intensities is passed. Several experimental VGM real-time devices have been constructed and the results of a level slicing experiment are presented. This device has the potential to perform a wide variety of real-time, parallel, optical processes.*

\*\*\*

We are investigating the feasibility of using the variable grating effect for nonlinear optical data processing. Separately the possible mechanisms responsible for the VGM are being investigated. Liquid crystals exhibit domain structures; these are particularly evident when the liquid crystal is in the form of a thin film or when it is sandwiched between planar electrodes. Domain structure, which manifests itself by periodic reorientation of the optical axis of the liquid crystal, may be seen when no external electric or magnetic fields are applied or when electrohydrodynamic or magnetohydrodynamic instabilities are induced by a field. In particular, a nematic-phase liquid crystal, sandwiched between electrodes spaced 12  $\mu\text{m}$  or less and with a static electric field normal to the electrodes, exhibit domains that appear as parallel structures. These domains extend along the direction of quiescent state alignment of the liquid crystal on the electrode surface, this alignment having been induced by rubbing or other appropriate methods. These domains have the unique property that they can act as phase diffraction gratings, the grating constant being a function of the applied voltage.

Cells were fabricated from plane electrodes that had been coated with ITO to provide a conductive surface. Mylar spacers were used, and cell parallelism was determined on an interferometer to be within one-half a fringe. Observations on domains were done with a polarizing microscope. A phase contrast microscope was also used, but produced no observably different results. Alignment on the surface was induced by rubbing or with an ion bombardment etch-alignment method.

VGM domains have previously been observed in planar cells.<sup>1,2,3</sup> We also observed these, but, contrary to the previous reports in the literature, we found the cell-spacing limit to be 12 rather than 6  $\mu\text{m}$ . Also contrary to these reports, the domains for static fields always are parallel to the quiescent-state alignment on the electrode surface. For alternating fields, the domains (commonly known as Williams domains) are perpendicular to the quiescent state alignment.

For alternating fields of 10 Hz or higher, the cells always showed Williams-type domains. These domains exist in a narrow range above the threshold voltage because, as the voltage is raised, increased flow within the cell, by causing turbulence, causes scattering to occur. This, and the very small variation in the spacing of domains, limits the utility of this mode in any practical device.

For frequencies below 10 Hz, a mixed-mode behavior is observed, with VGM- and Williams-type domains appearing alternately. The cells also exhibit severe scattering during the appearance of the Williams domains, especially as the frequency is raised.

For static fields, there is a large linear variation in domain spacing as a function of voltage. For the azoxy compound Merck NV in a 6.3- $\mu\text{m}$  cell, for example, the slope is ~8 lines/mm-V. For high-resistivity samples ( $10^{10}$   $\Omega/\text{cm}$ ), little or no dynamic scattering occurred even for voltages as high as five times the threshold. Figure 1 shows a series of views of a VGM cell taken through a polarizing microscope. The predominant apparent effect is a decrease in the period of the phase grating as voltage increases. Some of the

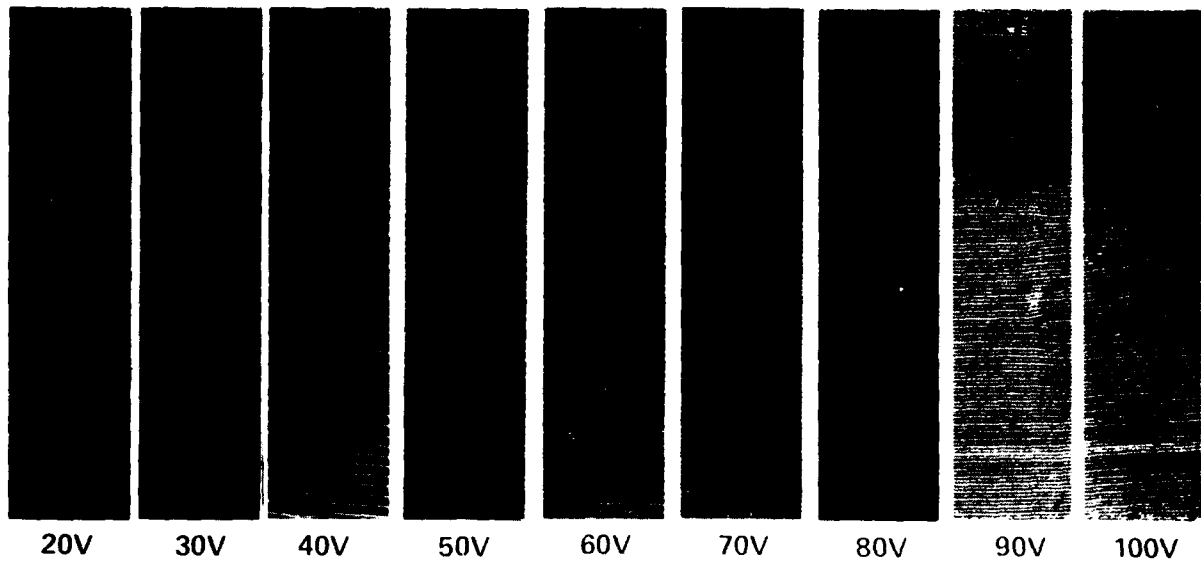


Figure 1. VGM viewed through polarizing microscope.

typical imperfections in the VGM device can also be noted in the photographs. There are places where two or more domains merge through arcs that, although small and not numerous, have the noticeable effect of degrading the diffraction patterns by smearing and arcing the points in Fourier space. The remedy for this is not yet known. Furthermore, inconsistency in the grating alignment within each picture and from picture to picture may be noted.

The diffraction patterns obtained from a typical VGM cell are shown in Figure 2. The light beam was not well collimated in these pictures, as can be noted from the size of the zero-order spot, but the pictures serve to demonstrate the general features of the diffraction, including the development of circular arcs in the higher voltage examples.

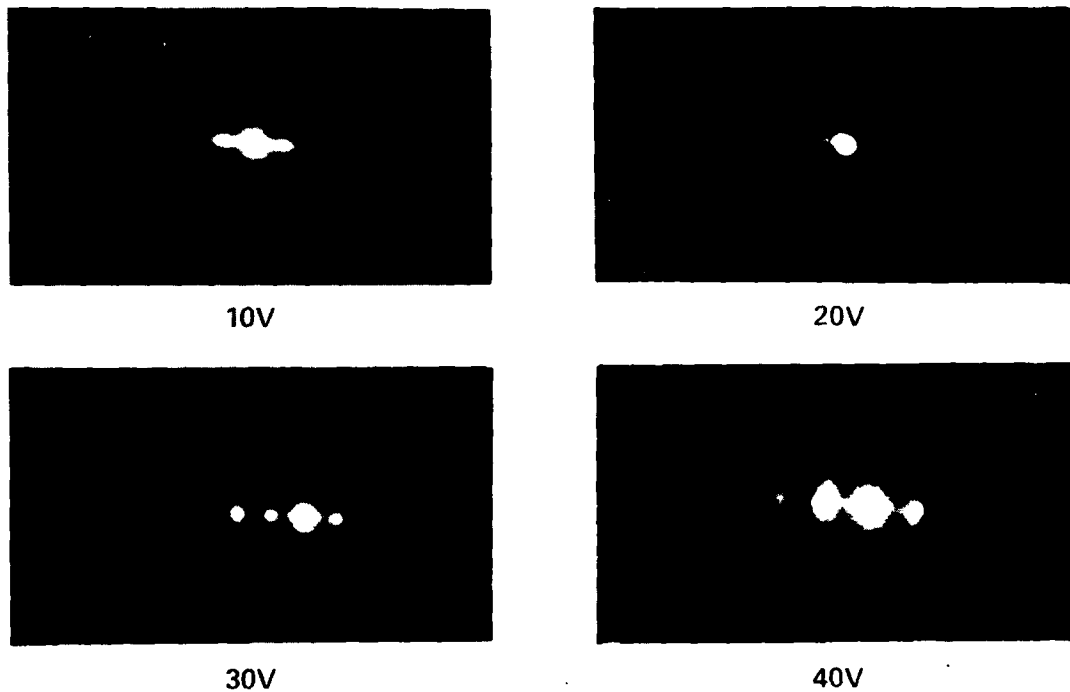


Figure 2. Diffraction patterns of a VGM cell.

The diffraction efficiency of the VGM cells is >25% in 1st order. The relative strengths of the orders show that the optical phase does not vary simply sinusoidally across the grating. Interesting polarization effects are sometimes noted where all the odd orders and even orders behave differently with variation of the polarization of the light.

Preliminary work has been done on the response time. For azoxies, when switched on to a voltage above threshold, Williams-type domains appear first, accompanied by some scattering. These domains then decay into the VGM-type domains by twisting through 90° from their original direction. The process requires 3 to 4 sec. For esters, the times were as great as 15 sec. Decay time appears to vary with cell thickness.

The quality of the domains (e.g., their parallelism and the direction along which they extend) appears to depend on surface treatment. Thus, when the ITO film is coated with SiO<sub>2</sub> deposited at a medium angle, the domains are no longer parallel but are randomly curled in a plane parallel to the electrode surface. The grating lines in the VGM lie parallel to the liquid-crystal director. The orientation of the liquid-crystal director is enforced only by the preparation of the surfaces of the electrodes. Although rubbing has proven to be satisfactory for test cells, a much more uniform homogeneous alignment can be obtained by ion-beam etching certain types of surfaces. Figure 3 shows the best quality of domains yet obtained.

We have studied the liquid-crystal parameters relating to VGM operation to find the most suitable liquid-crystal mixture for this application. Eleven different LCs have been tested and compared so far.

The VGM effect in nematic-phase LCs of negative dielectric anisotropy has been demonstrated with azoxy mixtures, such as Merck NP V.1,3,4. These yellow-colored eutectic mixtures from aromatic azoxy compounds absorb light in the UV and visible (below 420 nm) region of the spectrum, and they can undergo photodecomposition during long illumination. Other classes of LCs, such as phenyl benzoates, are stable to visible light with an absorption edge below 330 nm. Eutectic mixtures of these aromatic esters with varying average molecular lengths were studied for VGM under another AFOSR program (79M-0553/D7283-3). These same highly purified phenyl benzoate mixtures without dopants were tested for VGM operation and their response correlated with their average chain length, viscosity, anisotropy, index of refraction, and resistivity.

A cell was fabricated from ITO-coated, 0.5-in.-thick optical flats and a 6-μm Mylar spacer sandwiching the LC. The effect of dc voltage was observed with a polarizing microscope at 258x magnification for each LC mixture. The domain width  $d$  is inversely proportional to applied voltage according to:

$$d = \alpha/V$$

where  $\alpha$  is a constant that is dependent on the particular LC mixture. This relationship is best shown in Figure 4, where dc voltage versus grating period  $1/d$  for each eutectic is a straight line with a slope of  $\alpha^{-1}$ . The period of domain structure depends mainly on the sample thickness  $l$ , and less on other parameters according to<sup>5</sup>

$$d = 0.8(\beta/\rho k_{11})^{1/4} l ,$$

where

$\rho$  = density of LC

$k_{11}$  = elastic constant for splay

$\beta$  = viscosity coefficient.

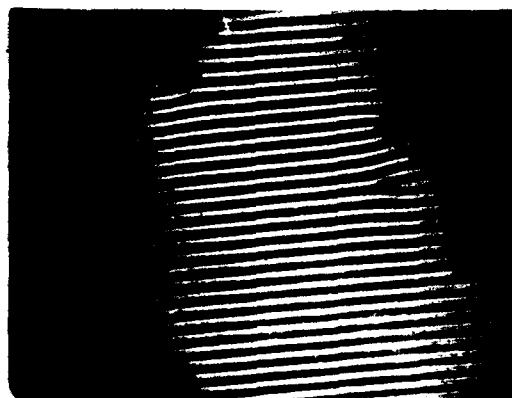


Figure 3. Domains in an etched cell. Magnification 100 times.

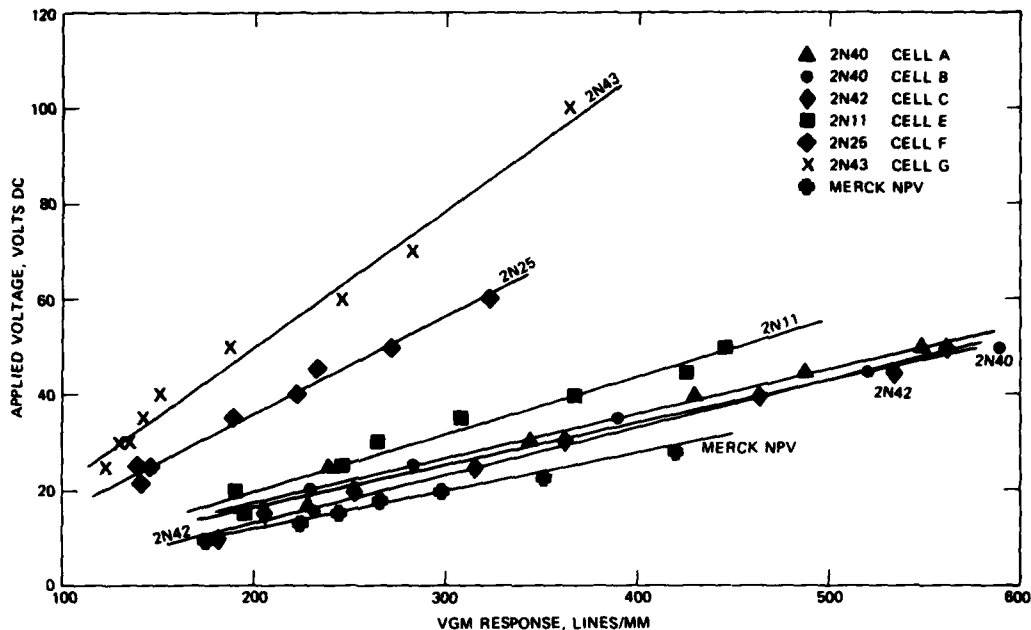


Figure 4. VGM voltage dependence for various LCs.

Some of these parameters suggest that, for the best VGM response (i.e., maximum grating period/volt):

- Average molecular length should be minimum
- Conductivity anisotropy should be high
- Large  $\Delta n$  is preferred
- Range of LC resistivity  $2 \times 10^{10}$  to  $1 \times 10^{11} \Omega\text{cm}$
- Not dependent on viscosity

Research was performed on the photoconductive layer for the VGM photoactive cell.

The structure of the present photoactivated device is shown schematically in Figure 5. It includes a sputter-deposited ZnS photoconductor, and a liquid-crystal layer. These are between indium-tin oxide (ITO), transparent electrodes that have been deposited on glass substrates. A low-voltage dc drive voltage is impressed across the electrodes.

The operating principle of the device is straightforward. The thin-film structure is designed to accept most of the drive voltage when the photoconductor is not illuminated; the portion of the voltage that falls across the liquid crystal is below the activation threshold of the liquid-crystal VGM effect. When light falls on the photoconductor, the photoconductor's impedance drops, thereby switching the voltage from the photoconductor onto the liquid crystal and driving the liquid crystal into its activated state. Thus, the photoconductor acts as a light-activated voltage gate. The high lateral impedance of the thin films causes there to be very little spreading of the light or of the associated liquid-crystal electrooptic effect. As a result, the light-activation process is a high-resolution process, and the device can accept photographic-quality images.

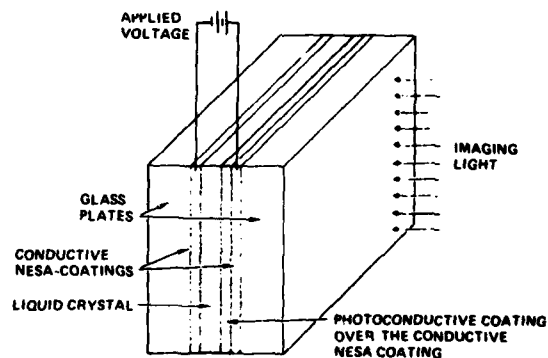


Figure 5. Schematic VGM cell.

# VARIABLE GRATING MODE LIQUID CRYSTAL DEVICE FOR OPTICAL PROCESSING

The VGM phenomenon is a dc electrohydrodynamic instability effect occurring in high-resistivity ( $\rho > 10^{10} \Omega\text{cm}$ ), pure liquid-crystal compositions. They require high-impedance photoconductor layers. Zinc sulfide photoconductor has been selected for the best impedance match with the LC. Unfortunately, its photosensitivity is in the blue and uv region of the spectrum, where the LC molecules are sensitive to photodecomposition.

The ZnS layer is deposited on conductive ITO electrodes by evaporation or ion-beam-sputtering methods. With the evaporation technique, we produced photoconductors of 1.5 to 5  $\mu\text{m}$  thickness, while the sputtered films were only 5,000 Å thick, highly transparent smooth surface layers. The evaporated 1.5 to 5  $\mu\text{m}$  ZnS photoconductors had a hazy, rough surface appearance causing difficulties in LC alignment parallel to the electrodes. It has been reported that vaporized ZnS causes homeotropic or tilted homeotropic orientation of the LC material.<sup>6</sup> Mechanical polishing of the evaporated photoconductors increased their transparency and surface uniformity, while polymer (PVA) coating the top of these ZnS layers, supplemented by additional surface treatment, resulted in good parallel alignment. Photosensitive devices were fabricated from the vapor-deposited and sputtered ZnS using ITO counter electrodes and 6- $\mu\text{m}$  spacers. The photoconductors were evaluated and compared by measuring the dark current and switching ratios of the VGM devices. The photojunctions sometimes observed can help to increase the effective switching ratio of current with and without illumination. In Figure 6, the behavior of one such junction is plotted. It resembles the behavior of two photojunctions back to back. At a certain bias, this cell crossed over through zero switching ratio (for the illuminations shown) and reversed to a negative ratio! A layer-by-layer study of the elements of the cells is being done to determine the nature of these junctions. From the results, for devices with switching ratios above 6, the dark current has to be less than  $6 \times 10^{-9} \text{ A-in}^{-2}$ , and this low dark current is obtained with sputtered as well as evaporated ZnS.

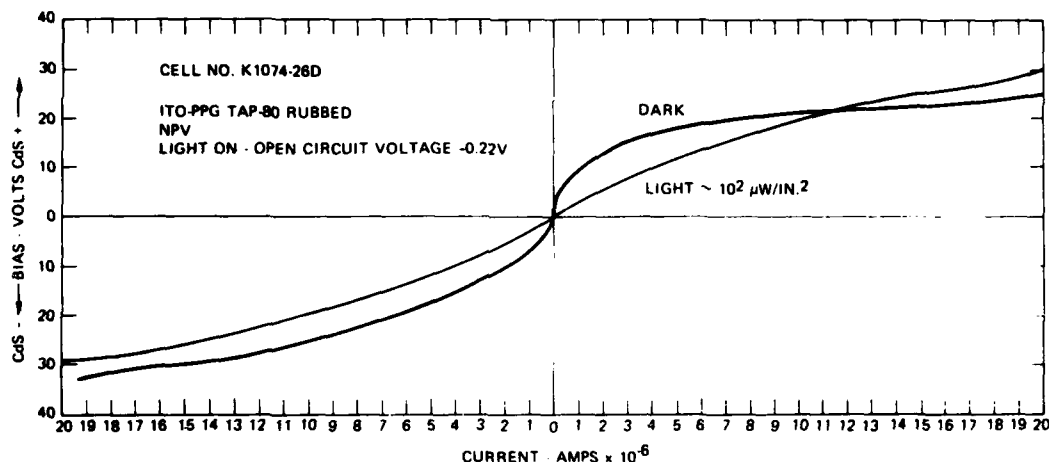


Figure 6. Junction effect in VGM cell.

VGM cells were studied with respect to edge effects on resolution and possible "spillover" of domains into adjacent unactivated areas. Electrodes were specially prepared by removing sections of the conductive coating by etching. A parallel plate cell was constructed such that there were conductive areas facing each other, either with conductive edges aligned or with a maximum overlap of 150  $\mu\text{m}$  of a conductive electrode over the nonconducting area. Cell spacing was 6.3  $\mu\text{m}$ , and the material was Merck NV. For alignment parallel to the edge when operating close to the threshold voltage, domains were parallel to the edge and within the active area. For higher voltages, there was fringe spillover by not more than one fringe spacing. For alignment perpendicular to the edge, domains appear to either terminate at the edge or to join with an adjacent domain. The quality of the edge behavior is shown in Figure 7.

The results indicate that a VGM light valve is a viable device requiring dc operation. Studies of the edge effects indicate that implementation of the VGM in an image-processing device should ultimately produce excellent resolution.

From the preliminary photosensitive devices fabricated using a ZnS photoconductor layer to achieve the high impedance needed, one cell was selected that aligned well and did not suffer the usual rapid deterioration seen in dc operation. This deterioration supposedly results from poisoning the LC by the diffusion of ions from the photoconductor. The cell was biased negatively on the photoconductor. This cell was protected as much as possible from short wavelength illumination although this was not entirely possible since ZnS requires blue to long UV for photoexcitation. This particular cell was constructed of a 5- $\mu$ m-thick evaporated ZnS layer that had been polished and then rubbed with surfactant polyvinyl alcohol. The 6- $\mu$ m-thick LC layer was made of Hughes 2N40 ester. The counter electrode was an ITO transparent layer treated with the same surfactant. The series impedance was measured to be  $\sim 3 \times 10^8 \Omega$ . With 160 V applied and with the maximum available illumination at 7.3 mW/cm<sup>2</sup> in the passband 410 to 550 nm, the periodicity of the VGM was calculated from the diffraction to be 588 lines/mm. The device threshold at this illumination was 21 V, corresponding to a grating periodicity of 103 lines/mm. The optical threshold at 160 V is  $\sim 50 \mu$ W/cm<sup>2</sup>, and the device appears saturated at 7.5 mW/cm<sup>2</sup>. Saturation behavior remains to be studied. With an image on the photoconductor surface of the device, a mapping into local intensity dependent periodicities is produced in the LC layer.

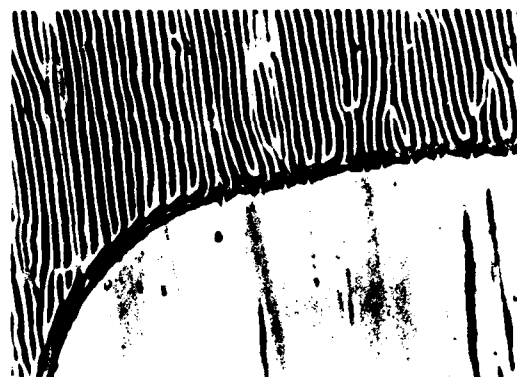


Figure 7. Behavior of domains near an edge. Magnification 100 times.

Intensities can be mapped, within the dynamic range of the device, monotonically into positions along a line in Fourier space by an optical transform. Departures from the line may be caused by imperfections in the alignment of the induced grating direction. The spatial positional information is coded into phase and sidebands in two dimensional Fourier space. A new parameter, the intensity, has thus been coded into Fourier space. Since the periods of the VGM are much finer than the periods encountered in the images to be processed, we are in a tractable situation, familiar in communications, where the carrier frequency is higher than the modulation frequencies. Optical filtering should produce a variety of linear and nonlinear image transformations. One such transform, isophote contouring (or level slicing) is described below.

For a first example of the use of the VGM device, we have successfully demonstrated level slicing of a continuous-tone image using simple Fourier filtering. Small circular annuli of varying radii were used to select particular intensities or level slices. Figure 8 shows a series of such slices. Figure 8(a) shows a positive print of the original image as photographed on the imaging screen. The negative was used in the experiments. Figure 8(b) shows a low-intensity level slice corresponding to a VGM periodicity of 120 lines/mm with  $\sim 3\%$  bandwidth. In Figure 8(c), another level, corresponding to 153 lines/mm, is shown. Figure 8(d), at 236 lines/mm illustrates an ambiguity not mentioned before. Weak second harmonics of the low-intensity image slice corresponding to 118 lines/mm can appear in the 236-lines/mm level slice. It should be possible to resolve this ambiguity by subtraction or by other schemes. In Figure 8(e), a broader slice of 11% bandwidth was taken centered about the level corresponding to 140 lines/mm. This picture may be compared with the previous slices and particularly with the slice shown in Figure 8(c). Finally, Figure 8(f) shows a very high intensity slice at 440 lines/mm of 10% bandwidth. Three gray levels may be seen simultaneously; these correspond to the superposition of three wide-intensity slices.

#### Acknowledgments

This project was sponsored by the Air Force Office of Scientific Research under grant AFOSR-77-3285 and Contract F49620-77-C-0080.

#### References

1. J.D. Margerum et al., Phys. Lett. 19, 216-218, October 1971.
2. W. Grenbel and V. Wolf, Appl. Phys. Lett. 19, 213-215, October 1971.
3. J.M. Pollack and J.B. Flannery, SID 76 Digest, pp. 143-145. University of Southern California Image Processing Institute Report 720, 30 September 1976.
4. P.K. Watson, J.M. Pollack and J.B. Flannery, "Liquid Crystals and Ordered Fluids, Vol. 3, p. 421, (1977).
5. I.G. Chistyakov and L.K. Vistin, Sov. Phys. Crystallogr. Vol. 19, No. 1, July-Aug (1974).
6. H. Kruger, H.F. Mahlim, and W. Raushcer, U.S. Pat. 4,112,157, 05 Sept. 1978.

VARIABLE GRATING MODE LIQUID CRYSTAL DEVICE FOR OPTICAL PROCESSING

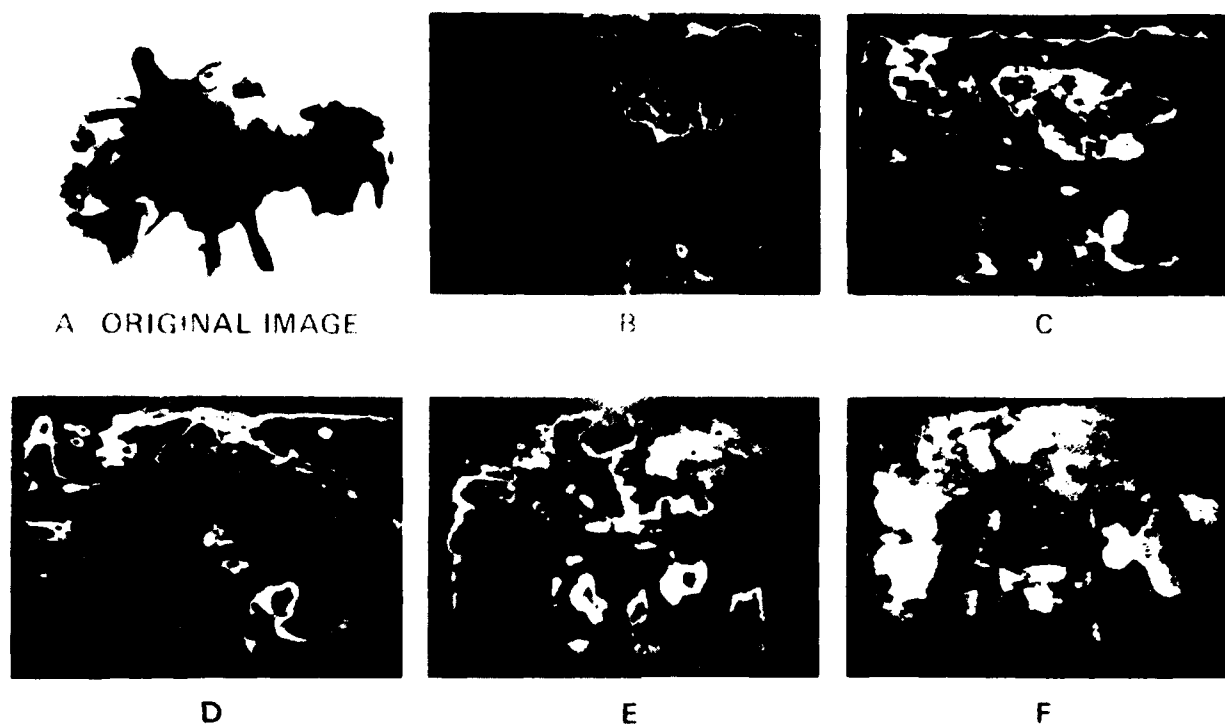


Figure 8. Level slicing with the VGM LCLV.

The VGM effect in nematic-phase liquid crystals of negative dielectric anisotropy has been previously studied, primarily with azoxy mixtures, such as Merck NP-V. These yellow-colored eutectic mixtures absorb light strongly in the near ultraviolet and blue (below 430 nm) region of the spectrum, and can undergo photodecomposition during extended illumination. We studied phenyl benzoate liquid crystal mixtures because they are colorless (strong absorption below 350 nm), are more stable to visible light exposures, and are more easily purified than the azoxy mixtures. Since we have been studying structural effects (particularly molecular length) on the anisotropic and dynamic scattering properties of a series of phenyl benzoate mixtures, we examined the VGM response of this series, as well as several other mixtures. The purpose was two-fold: (1) to select phenyl benzoate mixtures suitable for VGM studies in photoactivated devices, and (2) to look for correlations of structures or physical properties with the VGM effect. The materials studied are shown in Table 1. Their VGM characteristics are compared with some of their anisotropic properties in Table 2. The voltage dependence of their VGM domain grating frequency is shown in Figure 10. The general structure of the LC mixture component and a typical model are shown in Figure 11. The width  $d$  of the domain period (line pair) is inversely proportional to applied voltage, according to

$$d = \alpha/V ,$$

where  $\alpha$  is a constant that is dependent on the particular liquid crystal mixture. This relationship is illustrated in Figure 10, in which dc voltage as a function of grating frequency  $1/d$  for each eutectic mixture is a straight line with slope  $\alpha$ . Values of  $\alpha$  for various liquid crystal mixtures are given in Table 2. A smaller value of  $\alpha$  is preferred, since a smaller slope gives a larger range of spatial frequency for the VGM effect per unit of applied voltage. Thus, HRL-2N40 was chosen as the best of these ester liquid crystal mixtures for use in our studies of the photoactivated VGM device. The HRL-2N42 mixture is also of interest because its  $\alpha$  value is almost as low as that of HRL-2N40, and its viscosity is considerably lower.

Table 1. Composition of Some HRL Liquid-Crystal Mixtures.

11200-1

End Group Component		Mole Fraction in Mixtures							
RO	R'	2N42	2N43	2N44	2N46	2N48	2N11	2N40	2N25
CH <sub>3</sub> O	CH <sub>3</sub>	0.112	0.073	----	----	----	----	0.062	----
C <sub>2</sub> H <sub>5</sub> O	C <sub>3</sub> H <sub>7</sub>	0.222	0.148	----	----	----	----	0.129	----
C <sub>2</sub> H <sub>5</sub> O	C <sub>2</sub> H <sub>11</sub>	0.283	0.180	0.240	----	----	----	0.155	0.132
C <sub>4</sub> H <sub>9</sub> O	CH <sub>3</sub>	0.191	0.119	----	----	----	----	0.102	----
C <sub>4</sub> H <sub>9</sub> O	C <sub>3</sub> H <sub>7</sub>	0.192	0.117	0.160	0.120	----	----	----	----
C <sub>4</sub> H <sub>9</sub> O	C <sub>6</sub> H <sub>13</sub>	----	0.364	----	0.375	----	----	0.307	----
C <sub>6</sub> H <sub>13</sub> O	C <sub>3</sub> H <sub>7</sub>	----	----	----	----	0.249	----	----	----
C <sub>6</sub> H <sub>13</sub> O	C <sub>4</sub> H <sub>9</sub>	----	----	0.601	----	----	----	----	0.640
C <sub>6</sub> H <sub>13</sub> O	C <sub>5</sub> H <sub>11</sub>	----	----	----	0.504	0.331	----	----	----
C <sub>8</sub> H <sub>17</sub> O	C <sub>3</sub> H <sub>7</sub>	----	----	----	----	0.213	----	----	----
C <sub>8</sub> H <sub>17</sub> O	C <sub>6</sub> H <sub>13</sub>	----	----	----	----	0.207	----	----	----
RO	OR'								
C <sub>6</sub> H <sub>13</sub> O	OCH <sub>3</sub>	----	----	----	----	----	----	0.245	0.228
C <sub>4</sub> H <sub>9</sub> O	OC <sub>4</sub> H <sub>9</sub>	----	----	----	----	----	0.143	----	----
C <sub>4</sub> H <sub>9</sub> O	OC <sub>6</sub> H <sub>13</sub>	----	----	----	----	----	0.143	----	----
C <sub>4</sub> H <sub>9</sub> O	OC <sub>8</sub> H <sub>17</sub>	----	----	----	----	----	0.143	----	----
R	R'								
C <sub>4</sub> H <sub>9</sub>	CH <sub>3</sub>	----	----	----	----	----	0.571	----	----

Table 2. Liquid Crystal Anisotropic Properties and VCM Response

11200-2

Class and Number	Nematic Range		Average Mixture Component Length, Å	Viscosity at 25°C, (cP)	$\Delta n$ at 22°C & 589 nm	AC-Resistivity $\rho_1 \times 10^{-10}$ (ohm-cm)	$\Delta c$ at 25°C & 5 kHz	VCM Characteristics <sup>a</sup>		
	mp, °C	clpt, °C						$V_{th}$ (volts)	Width, $d_{th}$ (μm)	Slope, $\alpha$ (Vmm/lp)
Azoxy										
Merck NP-V	-5	73	18.69	24.9	0.290	2.0	-0.2	10	8.5	0.082
RO-R' Esters <sup>c</sup>										
HRL-2N42	5	58	20.39	32.6	0.162	6.1	-0.22	10	5.4	0.099
HRL-2N43	-6	52	22.37	36.5	0.148	7.2	-0.25	25	8.1	0.287
HRL-2N42/48	2	57	23.36	36.9	0.140	33.0	-0.29	35	5.6	0.340
HRL-2N44	-8	51	24.31	38.1	0.136	10.0	-0.30	b	---	---
HRL-2N46	16	55	25.92	39.8	0.135	21.0	-0.30	b	---	---
HRL-2N48	18	56	27.14	44.5	0.134	23.1	-0.33	b	---	---
RO-OR' Components <sup>d</sup>										
HRL-2N11	13	47	22.26	43.8	0.133	2.8	-0.05	15	5.1	0.122
HRL-2N40	0	58	22.68	46.9	0.151	8.5	-0.28	16	4.3	0.089
HRL-2N25	0	56	24.48	48.5	0.139	11.0	-0.40	21	7.1	0.203

<sup>a</sup> The threshold voltage,  $V_{th}$ , is the lowest voltage at which the width of the domain period,  $d_{th}$ , was easily measured in cells with 6 μm spacers.

<sup>b</sup> No VCM observed up to 100 Vdc.

<sup>c</sup> RO-R' refers to 4-alkoxyphenyl 4-alkylbenzoate esters.

<sup>d</sup> RO-OR' refers to 4-alkoxyphenyl 4-alkoxybenzoate esters. The 2N11 mixture has a R-R' component, 4-butylphenyl 4-toluate, and no RO-R' components.

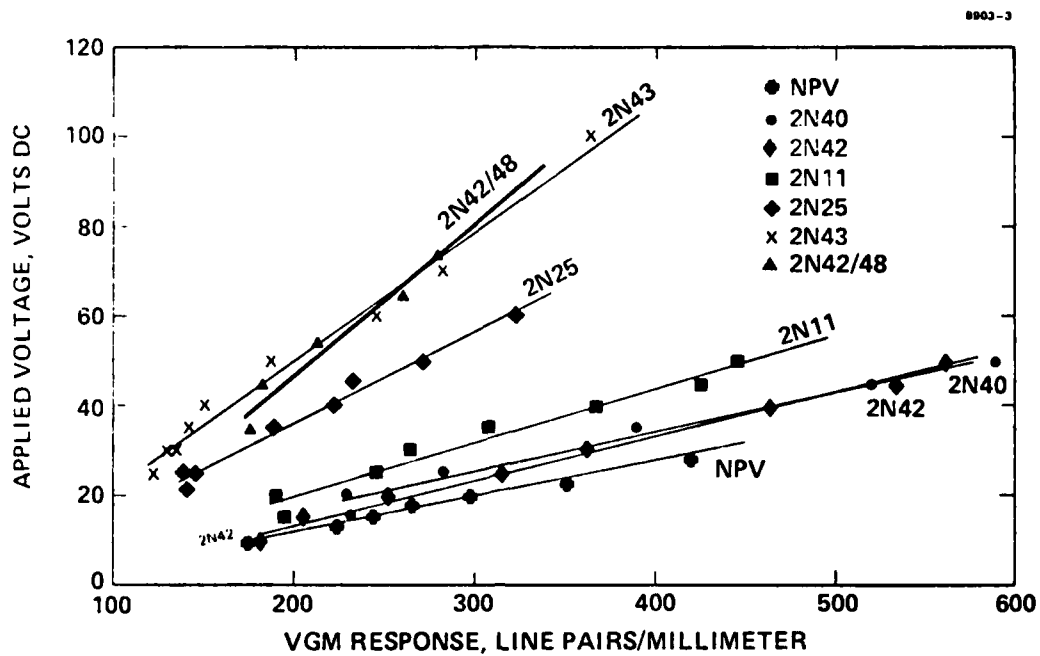
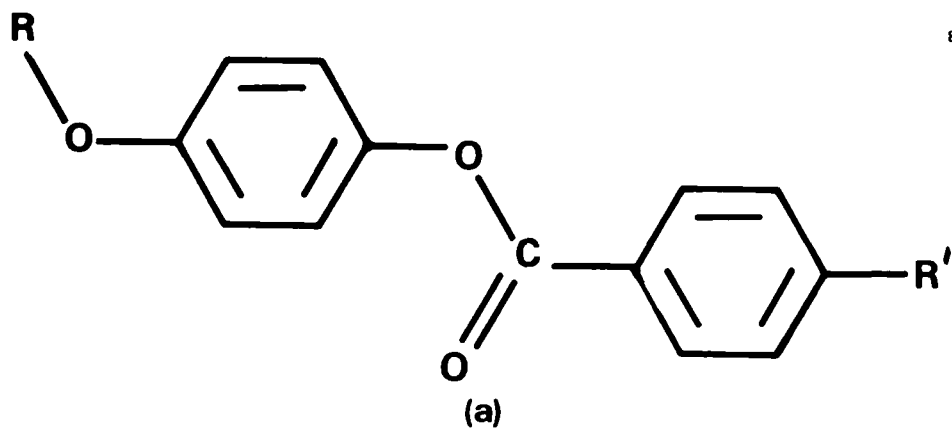
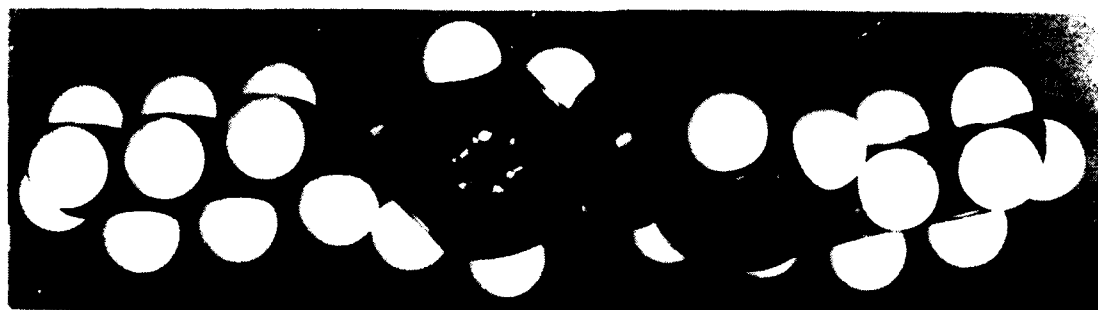


Figure 10. VGM voltage dependence for various liquid crystals.



M13113

9248-1



(b)

Figure 11. Liquid crystal mixture components.

There is an interesting correlation between the VGM effect and the average molecular length of the mixtures in the RO-R' ester series in Tables 1 and 2. As their length increases (due to longer alkyl end groups), the  $V_{th}$  and  $\alpha$  of the first three mixtures (2N42, 2N43, and 2N42/48) increase. The longer length mixtures (2N44, 2N46 and 2N48) do not show VGM effects. Since the dielectric anisotropy ( $\Delta\epsilon$ ) is reported to have a large effect on VGM, it may be the change of  $\Delta\epsilon$  with average length that causes these results. In this series, the  $V_{th}$  increases as  $\Delta\epsilon$  becomes more negative (with increasing length), and no VGM is observed when  $\Delta\epsilon$  is -0.3 and more negative. This is similar to the VGM effects reported by Barnik et al. for a much wider range of  $\Delta\epsilon$ . In a more complex series of phenyl benzoate mixtures (containing four different classes of end groups) they found that  $V_{th}$  increased as  $\Delta\epsilon$  became more negative, and they also reported a critical value of  $\Delta\epsilon = -0.3$ . However, the critical value of  $\Delta\epsilon$  apparently varies with composition of the end group classes used since our 2N25 mixture of RO-R' and RO-OR' esters shows VGM, and has  $\Delta\epsilon = -0.40$ . Our latter group of three mixtures (2N11, 2N40 and 2N25) also shows a general trend of increased  $V_{th}$  with more negative  $\Delta\epsilon$ . The effect of  $\Delta\epsilon$  appears to be less significant in these mixtures than in the RO-R' series, but it should be noted that the 2N11 mixture is quite different in composition from the other two mixtures.

To model the molecular configuration in the VGM effect, experiments on the intensity and polarization states of the VGM diffraction orders have been performed as a function of input polarization state. The results can be summarized briefly as follows. With linear input polarization the odd diffraction orders are polarized linearly parallel to the VGM domains and their intensity is directly related to the parallel component of the input polarization. The even diffraction orders are linearly polarized with a  $180^\circ$  relative phase shift induced between the polarization components parallel and perpendicular to the VGM domains. These Fourier space results are well correlated with high resolution polarizing microscope studies in real space of an electrically activated VGM cell. The experiments have enabled us to produce a model of the liquid crystal director pattern within the domains.

A static model of the VGM has been developed which qualitatively reproduces the observed diffraction phenomena. A computer program has been implemented to see how well predictions from the model match the measured diffraction efficiencies. Our model assumes that the liquid crystal director orientation rotates both in the plane of the liquid crystal device, and out of the plane as one moves through one period of the grating structure. The director thus sweeps out a cone in one period of the grating. The axis of the cone coincides with the director axis when no voltage is applied. The cross section of the cone orthogonal to the axis of the cone is, in general, elliptical in shape.

Using the maximum value of the two rotation components of the director as parameters, the model predicted diffraction intensities for the first five orders, which agreed with the measured value with less than ten percent error. In fact, this error was only slightly higher than the measurement error.

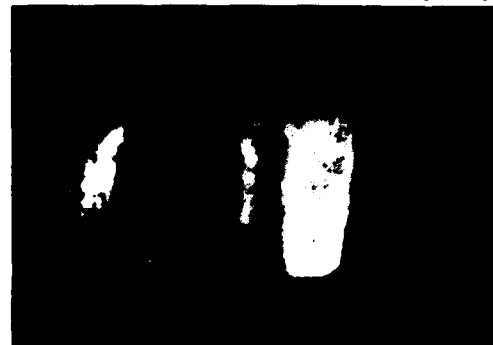
Work is in progress to refine the model, and to perform additional experiments to identify additional aspects of the model which are not uniquely specified at this point.

## 2. Applications

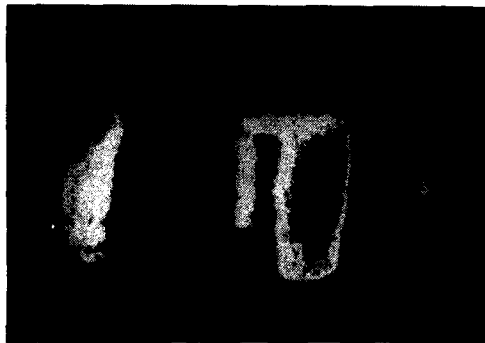
A new generation of improved VGM photoactuated devices was successfully fabricated after the publication of the above inserted paper. By careful attention to processing details, and the utilization of high optical quality 1/10 wave flats, a great improvement in uniformity, freedom from defects, and resolution was achieved. The photoconductor was vapor deposited with ZnS, 5  $\mu\text{m}$  thick. Three of these devices were selected to perform the non-linear optical process of "level-slicing" or isophotometric contouring of images. These devices were aligned by mechanical rubbing, with resulting traces that can be seen in the zeroth order as a background noise. The resolution of the system employed here is approximately 6 lines/mm. Figure 12 shows a sequence of level slices using a 6- $\mu\text{m}$ -thick LC VGM cell. The objects include a cube, barely visible on the left; a cylinder; and a sphere on the right. The filter for level-slicing with the VGM device is simply a slit in Fourier space, positioned at the appropriate mapped position of the desired intensity level. Figure 13 shows a similar sequence for a 12- $\mu\text{m}$ -thick



(a)



(b)



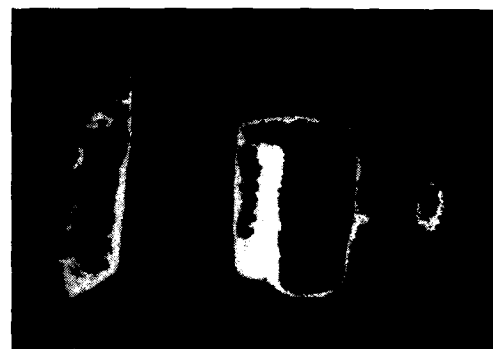
(c)



(d)



(e)



(f)

Figure 12. Level slicing with 6  $\mu$ m VGM cell, cylinder.

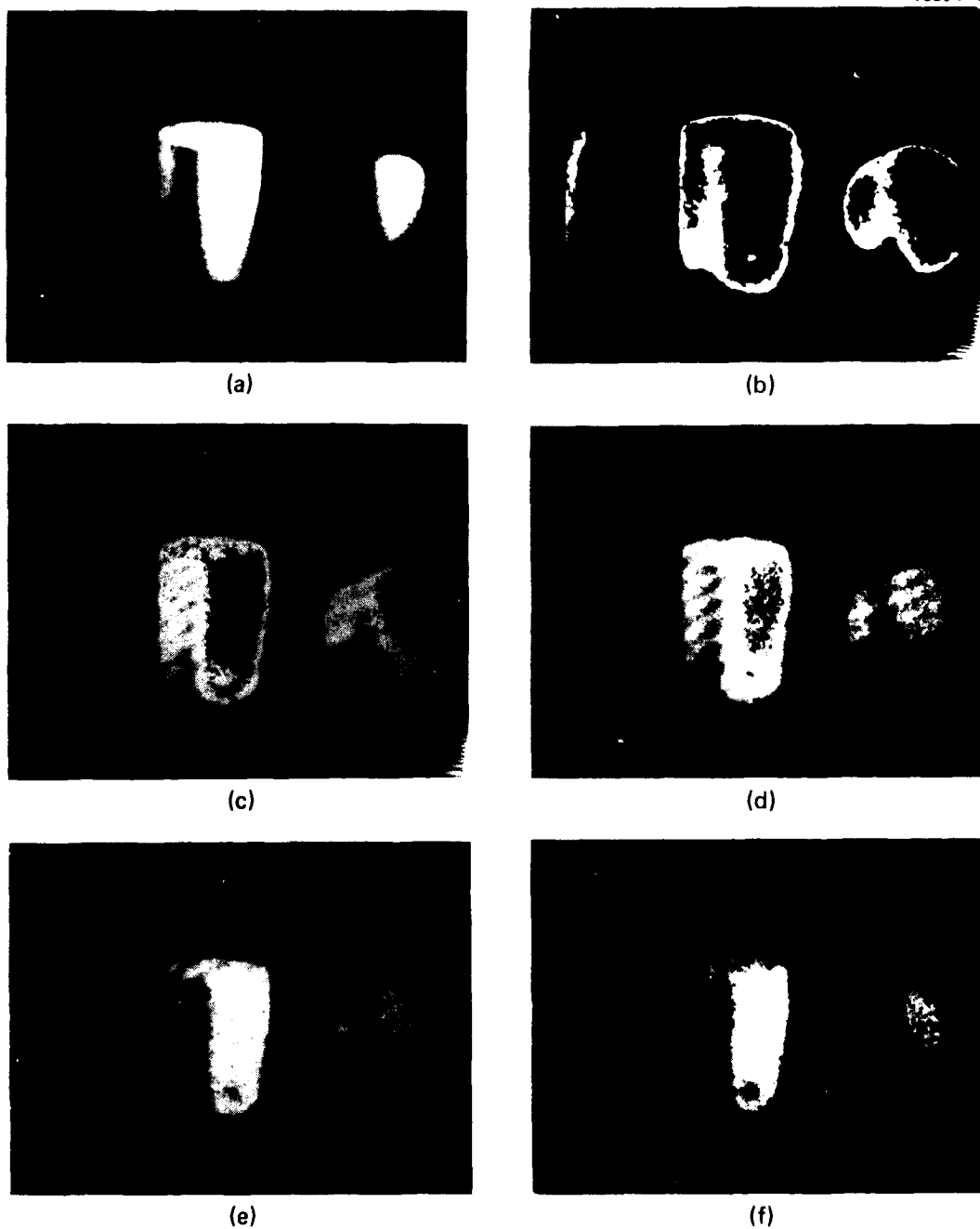


Figure 13. Level slicing with 12 um VGM cell, cylinder.

liquid crystal VGM device. Spurious interference fringes can be seen in Figures 13(d) and 13(e) resulting from reflections in the apparatus. In these level-slicing results, a far greater cell uniformity and resolution can be seen than in that which was reported earlier.

Many new applications for the VGM device have been investigated. Besides the direct implementation of nonlinear functions such as level slicing, we have shown that all positive and negative digital logical functions can be implemented readily. These functions or operations can be conceived of as special cases of nonlinear functions. The VGM device, which transforms intensities to positions is easily employed in these applications, with minimal coherence requirements, flexible programmability, and level restoration. We include here two recent publications which provide a concise summary of the applications of the VGM device to optical logic and optical computing.

## Optical computing with variable grating mode liquid crystal devices

B. H. Soffer, D. Boswell, A. M. Lackner

Hughes Research Laboratories, 3011 Malibu Canyon Road, Malibu, California 90265

P. Chavel, A. A. Sawchuk, T. C. Strand, A. R. Tanguay, Jr.

Image Processing Institute, University of Southern California, Los Angeles, California 90007

### Abstract

A liquid crystal device that performs a two-dimensional intensity-to-spatial frequency conversion has been developed for use as an optical transducer. When such a device is used as the input transducer in an optical filtering arrangement, image intensity levels can be easily manipulated via Fourier plane filters. This variable input intensity-output intensity transfer function has numerous potential applications in image processing. Implementation of a variable level slice operation is discussed and experimental results presented. The VGM LCLV device is also particularly well adapted to performing binary logic operations on 2-D images. This application is discussed, and results demonstrating the implementation of common logic operations are presented.

### Introduction

One of the primary concerns in the fields of optical image processing and optical computing is the desire for a wider range of real-time input transducers to meet the special requirements of various processing schemes. Variable-grating-mode (VGM) liquid crystal devices offer a radically new approach to the problem of optical transducers<sup>1</sup>. The basic function of the VGM device is to perform an intensity to spatial frequency conversion. This is done simultaneously over a two-dimensional image field so that the intensity variations of an image are converted to local spatial frequency variations in a phase grating structure within the liquid crystal layer. Due to the intensity-to-spatial frequency conversion thus performed, a standard spatial filtering system can be used to manipulate the VGM spatial frequencies and thus the input intensities. In this paper we describe two basic applications of the VGM device: nonlinear processing of continuous tone images and optical logic operations on binary images. The VGM liquid crystal light valve has many advantages for both of these processes.

The ability to perform arbitrary point nonlinearities over two-dimensional images greatly increases the flexibility of optical processing systems<sup>2</sup>. In the past few years several different approaches to the problem of implementing generalized nonlinearities have been investigated<sup>3</sup>. These have included halftone screen techniques<sup>3,4,5,6</sup> nonlinear devices<sup>7,8</sup>, feed back methods<sup>9</sup>, and a variable level slice<sup>10</sup> among others. The main advantage of the VGM approach over previous methods is the ease of programming the functional nonlinearity desired for a given image transformation. This is done simply by changing the transmittance distribution of the spatial filter in the optical processing system. The spatial filter is relatively low resolution and need only have a space-bandwidth product equal to the number of gray levels to be processed independent of the space-bandwidth product of the input image.

The same programmability advantage applies to the implementation of binary logic operations. One device can be used to implement any of the common logic operations (AND, OR, XOR, and their complements) by simply changing a Fourier plane filter. Previously described optical logic systems were "hardwired" to perform specific operations<sup>11,12,13</sup>, and in most cases one or more logic functions proved difficult or cumbersome to implement.

A second major advantage of the VGM system is the possibility for level restoration at each stage in order to provide required noise immunity. This capability has been lacking in other numerical processing systems where noise accumulates in cascaded stages.

It should perhaps be pointed out that considerable effort has been directed toward using integrated optics for logic elements<sup>14,15,16</sup>. This approach is inherently one-dimensional and does not fully exploit the advantages available to fully parallel two-dimensional optical processing algorithms.

In the following we first describe the basic principles of operation of the VGM device. Then we discuss in more detail how it can be used for nonlinear processing of images and some of the limitations of device performance. A variable level slice experiment is described as an example of nonlinear processing. Next, the application of the VGM device to logic operations is introduced and some preliminary experimental results are presented.

## OPTICAL COMPUTING WITH VARIABLE GRATING MODE LIQUID CRYSTAL DEVICES

### VGM device description

The primary active element of the variable grating mode liquid crystal device is a thin layer of liquid crystal that is observed to form periodic stripe domains in the presence of an applied voltage<sup>1</sup> as shown in Fig. 1a. The formation of the domains results in a phase grating characterized by a spatial frequency that depends on the magnitude of the voltage across the liquid crystal layer. The grating period can be optically controlled by placing a two-dimensional photoconductive layer in series with the layer of liquid crystal.

The structure of the present photoactivated device is shown schematically in Fig. 1b. It includes a sputter-deposited ZnS photoconductor, and a liquid-crystal layer. These are sandwiched between indium-tin oxide (ITO) transparent electrodes that have been deposited on glass substrates. A low-voltage dc drive voltage is impressed across the electrodes.

The operating principle of the device is straightforward. The thin-film structure is designed to accept most of the drive voltage when the photoconductor is not illuminated; the portion of the voltage that falls across the liquid crystal is below the activation threshold of the liquid-crystal VGM effect. When light falls on the photoconductor, the photoconductor's impedance drops, thereby switching the voltage from the photoconductor onto the liquid crystal and driving the liquid crystal into its activated state. Thus, the photoconductor acts as a light-activated voltage gate. The high lateral impedance of the thin film causes there to be very little spreading of the photoconductivity or of the associated liquid-crystal electrooptic effect. As a result, the light-activation process is a high-resolution process, and the device can accept photographic-quality images.

### Nonlinear processing of continuous valued signals with the variable grating mode liquid crystal device

The VGM liquid crystal device can be considered to be an intensity-to-spatial frequency converter capable of operating on two-dimensional images. The intensity-to-spatial frequency conversion allows the implementation of arbitrary point nonlinearities with simple Fourier plane filters. As discussed above, when an input image illuminates the photoconductor surface of this device the intensity variations of the input image change the local grating frequency. If coherent light is utilized to Fourier transform the processed image, different spatial frequency components (corresponding to different input intensities) of the encoded image appear at different locations in the Fourier plane as shown in Fig. 2a. Thus, by placing appropriate spatial filters in this plane it is possible to obtain different transformations of the input intensity in the output plane as depicted in Fig. 2b. This figure describes the variable grating mode nonlinear processing graphically. The input intensity variation is converted to a spatial frequency variation by the characteristic function of the VGM device (upper right-hand quadrant). These variations are Fourier transformed by the optical system and the spectrum is modified by a filter in the Fourier plane (upper left-hand quadrant). Finally, a square-law detection produces the intensity observed in the output plane (lower left-hand quadrant). Considered together, these transformations yield the overall nonlinearity (lower right-hand quadrant). Design of a proper spatial filter for a desired transformation is a relatively easy task. For example, a level slice transformation requires only a simple slit that passes a certain frequency band or bands. A mathematical formulation of nonlinear processing utilizing the VGM device is presented in the next section.

### Variable phase grating analysis

Consider a phase grating (periodic array of phase shifting elements) extending to infinity in both the x and y directions. Let  $g(x,y)$  be the complex amplitude transmittance of the phase grating. Since the grating extends to infinity we can assume that  $g(x,y)$  is a periodic function of x and write it as a Fourier series expansion

$$g(x,y) = \sum_{n=-\infty}^{\infty} c_n \exp(j2\pi nx/L) \quad (1)$$

where

$$c_n = \frac{1}{L} \int_0^L g(x,y) \exp(-j2\pi nx/L) dx \quad (2)$$

and L is the period of the grating. Because we assume that the grating extends to infinity in the y-direction,  $g(x,y)$  is not an explicit function of y.

For the case of a uniform input intensity distribution and a Fourier plane filter  $H(f_x, f_y)$  which transmits only the first diffraction order, it can be easily shown that the output intensity,  $I_0$ , resulting from the inverse Fourier transform is

$$I_0(x, y) = |c_1 H(\frac{1}{L}, 0)|^2 \quad (3)$$

where  $H(\frac{1}{L}, 0)$  is the filter amplitude transmittance at the first diffraction order of the VGM grating with period  $L$  and  $c$  is a constant. Thus the output intensity is directly related to the variation in the filter transmittance as a function of spatial frequency.

Using the above analysis, the processing limitations of the VGM device can be estimated. The fundamental question to be answered is how large the smallest picture element, or pixel, must be with respect to the VGM grating frequency.

Suppose that the usable spatial frequency range over which the VGM device can operate is  $\delta v_0$ . To avoid crosstalk from higher diffracted orders the VGM device can only be operated between the first diffraction order and the next non-zero harmonic of the lowest fundamental frequency. Experiments indicate that the second harmonic can be eliminated by a polarizing filter so that the third harmonic is the next non-zero component. However, in the subsequent derivation it is assumed that the second order sets the limiting frequency for a "worst case" calculation. If the lowest frequency used is denoted by  $v_0$  then the usable frequency range is

$$\delta v_0 = 2v_0 - v_0 = v_0 \quad (4)$$

as shown in Fig. 3. If the number of intensity levels that must be distinguished is  $N$ , then the Fourier transform of any one aperture represented by  $2\Delta v$  in Fig. 3 must be contained within a region of width  $v_0/N$  in the Fourier plane. So we must have

$$2\Delta v \leq v_0/N. \quad (5)$$

If the pixel width is  $b$ , then the width of its Fourier transform is  $2/b$ , which implies that

$$2\Delta v = \frac{2}{b} \quad (6)$$

Combining Eq. (5) and (6) we have

$$\frac{2}{b} \leq v_0/N \quad (7)$$

or

$$bv_0 \geq 2N. \quad (8)$$

This relation thus requires that the pixel size contains  $2N$  periods of the lowest grating frequency if  $N$  grey levels are to be processed. For example, if  $v_0 = 200$  cycles/mm and  $N = 50$ , then each pixel must have a size  $b = 0.5$  mm. Thus if the device has a 50 mm square area a 100 x 100 pixel image could be processed with 50 defined grey levels.

#### Demonstration of a level slice function with the VGM device

In this experiment the ability of the VGM device to generate a level-slice nonlinearity is demonstrated. The experimental setup is shown in Fig. 4. The input picture is illuminated by an arc lamp source and imaged onto the photoconductor surface of a VGM device which initially has a uniform phase grating structure due to a dc bias voltage. The grating period is locally modulated by the input picture intensity, and this modulation is mapped into a position along a line in the spatial filter plane. A red filter ensures that only the readout laser beam enters the coherent optical processor. Small circular annuli of varying radii are used to pass certain spatial frequency bands. This in effect allows only prescribed input intensity ranges to appear in the output. Figure 5 shows both the input and level sliced output pictures. Figure 5a shows a positive print of the original image as photographed on the imaging screen. A negative of the original was used in the experiments. Figure 5b shows a low intensity level slice corresponding to a VGM periodicity of 120 lines/mm with approximately 3% bandwidth. In Fig. 5c another level, corresponding to 153 lines/mm, is shown. Figure 5d at 236

## OPTICAL COMPUTING WITH VARIABLE GRATING MODE LIQUID CRYSTAL DEVICES

lines/mm, illustrates the interference from second harmonics. Weak second harmonics of the low-intensity image slice corresponding to 118 lines/mm can appear in the 236 lines/mm level slice. In Fig. 5e, a broader slice of approximately 11% bandwidth was taken centered about the level corresponding to 140 lines/mm. This picture may be compared with the previous slices and particularly with the slice shown in Fig. 5c. Finally, Fig. 5f shows a very high input intensity slice at 440 lines/mm of 10% bandwidth. Three grey levels may be seen simultaneously; these correspond to the superposition of three broad intensity slices.

### VGM implementation of logic functions

To see how the VGM device can be used to implement logic operations, one need only realize that the function of a logic circuit can be represented as a simple binary nonlinearity. The input-output characteristics of the common logic functions are shown in Fig. 6. The input in these figures is assumed to be the simple arithmetic sum of the two input logic levels. Thus NOT is simply a hard-clipping inverter, AND and OR are hardclippers with different thresholds and XOR is a level slice function. Any spatial light modulator or optical processing system which can produce these nonlinearities can be used for implementing combinatorial logic. Furthermore, if the system allows feedback to be readily introduced, sequential or latching logic can also be implemented.

The VGM device is well suited to implementing these nonlinearities. With the VGM approach, nonlinearities are obtained using a Fourier plane filter whose transmittance variation in one-dimension is essentially a plot of the desired nonlinearity. Thus arbitrary nonlinearities are easily produced and changed. For logic operations the situation is quite straightforward. Since the nonlinearities associated with logic operations are binary functions, they can be implemented with simple slit apertures, i.e., 0 or 1 transmittance values. Such binary filters are the simplest filters to implement. A second feature of the VGM technique that is especially suitable for logic processing is that the input and output are physically separate beams. The input beam modulates a photoconductor; concurrently the image is read out with a second beam. This separation of input and output provides for the possibility of restoring the output levels to the 0 and 1 values even if the input levels are not exactly correct. This feature is essential to the production of a reliable logic system that is immune to noise and systematic errors in the levels. Electronic logic elements possess such level restoring capability, but currently proposed optical logic schemes lack this essential characteristic.

Two further aspects of logic operations which are advantageous for optical implementation purposes are the facts that logic operation input levels are discrete, and that only a small number (2-4) of distinguishable levels are required. The existence of discrete input levels implies that the nonlinearities need not have the exact forms shown in Fig. 6. In particular the transition regions need not be perfectly sharp thresholds since the input values are presumed not to occur within the transition regions in any event. The fact that only a few levels need be distinguished implies that the grey-level resolution requirements for the system are minimal.

The operations discussed above are the basic combinatorial logic functions. However, sequential logic may also be implemented with appropriate feedback, i.e., imaging the output plane onto the input plane (which can be accomplished with incoherent illumination). However, with the present VGM transmission devices there is a problem of separating the read and write functions in a feedback system since their wavelengths must be identical.

### Experimental results of logic implementation

A series of experiments were conducted to demonstrate the fundamental logic functions. The experimental setup of Fig. 7 was used. Two input fields were superimposed at the VGM plane along with a bias illumination. The total illumination intensity on the photoconductor of the VGM device was thus the sum of the two input intensities and the bias intensity. The input illumination was a filtered high-pressure mercury arc lamp. The bias illumination was provided by a collimated tungsten bulb source. The VGM device was read out in transmission using a HeNe laser. A filter was placed in the Fourier plane to select the desired diffraction orders for each logic function.

For these experiments, the inputs consisted of one vertical rectangular aperture and one horizontal aperture. When these were superimposed along with the bias, a square image was formed with the four quadrants having the intensity levels shown in Fig. 8. This image corresponds to the logic truth table shown. Thus the output images have intensity levels determined by the truth table associated with the desired logic function. The logic functions AND, OR, XOR and their complements were implemented sequentially as shown in Fig. 9 by altering only the Fourier plane filter. Imperfections visible in the output plane data arise from defects in the cell structure of the VGM device employed in these

experiments. Investigations on VGM device improvements, limitations, processing speed and pixel uniformity are in progress.

#### Conclusion

We have described a new type of optical transducer, the variable-grating-mode (VGM) liquid crystal device which operates by providing an intensity-to-spatial frequency conversion. It has been demonstrated theoretically and experimentally that this device can be used for implementing arbitrary nonlinearities on continuous tone images, and can be employed to perform combinatorial logic operations on binary images. The VGM approach has several advantages over other techniques. Principal among these advantages is the flexibility of the device inherent in its functional programmability, which may be exercised at will merely by changing a low-resolution spatial filter.

#### Acknowledgements

The authors acknowledge many useful discussions with A. Armand. This research was supported by the Air Force Office of Scientific Research, Electronics and Solid State Sciences Division, under Grant AFOSR-77-3285 at USC and Contract F49620-77-C-0080 at Hughes Research Laboratories.

#### References

1. B.H. Soffer et al., "Variable Grating Mode Liquid Crystal Device for Optical Processing," Proceedings SPIE 1980 Los Angeles Technical Symposium, Vol. 218, Los Angeles, February 1980 (to be published).
2. J.W. Goodman, "Operations Achievable with Coherent Optical Information Processing Systems," Proc. IEEE, Vol. 65, pp. 29-38 (1977).
3. A. Armand, "Real-time Nonlinear Optical Information Processing," (Ph.D. Thesis) USC/PI Report 880, Image Processing Institute, University of Southern California, Los Angeles, California 90007 (1979).
4. H. Kato and J.W. Goodman, "Nonlinear Filtering in Coherent Optical Systems Through Half-tone Screen Processes," Appl. Opt. Vol. 4, pp. 1813-1824 (1975).
5. H.-K. Liu, J.W. Goodman and J. Chan, "Equidensitometry by Coherent Optical Filtering," Appl. Optics, Vol. 15, pp. 2394-2399 (1976).
6. A. Armand, A.A. Sawchuk, and T.C. Strand, "Nonlinear Optical Processing with Half-tones: Accurate Predictions for Degradation and Compensation," submitted to Appl. Opt.
7. A. Armand, et al., "Real-time Optical Analog-to-Digital Conversion," Optics Letters, Vol. 5, p. 129 (1980).
8. A. Tai, T. Cheng, F.T.S. Yu, "Optical Logarithmic Filtering Using Inherent Film Nonlinearity," Appl. Opt., Vol. 16, pp. 2559-2564 (1977).
9. B.J. Bartholomew and S.H. Lee, "Nonlinear Optical Processing with Fabry-Perot Interferometers Containing Phase Recording Media," Appl. Opt., Vol. 19, p. 201 (1980).
10. J.D. Michaelson, and A.A. Sawchuk, "Nonlinear Optical Processing Using Liquid Crystal Light Valves," Proc. SPIE 1980 Los Angeles Technical Symposium, Vol. 218, Los Angeles, February 1980 (to be published).
11. R.A. Athale and S.H. Lee, "Development of an Optical Parallel Logic Device and Half-adder Circuit for Digital Optical Processing," Opt. Eng., Vol. 18, pp. 513-517 (1979).
12. S.A. Collins, Jr., U.H. Gerlach and Z.M. Zakman, "Optical Feedback for Generating Arrays of Bistable Elements," Proc. SPIE on Optical Processing Systems, Vol. 185, pp. 36-41 (1979).
13. D.H. Schaefer and J.P. Strong, III, "Tsc Computers," Proc. IEEE, Vol. 65, pp. 129-138 (1977).
14. L. Goldberg and S.H. Lee, "Integrated Optical Half-adder Circuit," Appl. Opt., Vol. 18, pp. 2045-2051 (1979).
15. S.M. Jensen, "High-Speed Optical Logic Devices," Proc. SPIE 1980 Los Angeles Technical Symposium, Vol. 218, Los Angeles, February 1980 (to be published).
16. E. Garmire, "Review of Integrated Optical Bistable Devices," Proc. SPIE 1980 Los Angeles Technical Symposium, Vol. 218, Los Angeles, February 1980 (to be published).

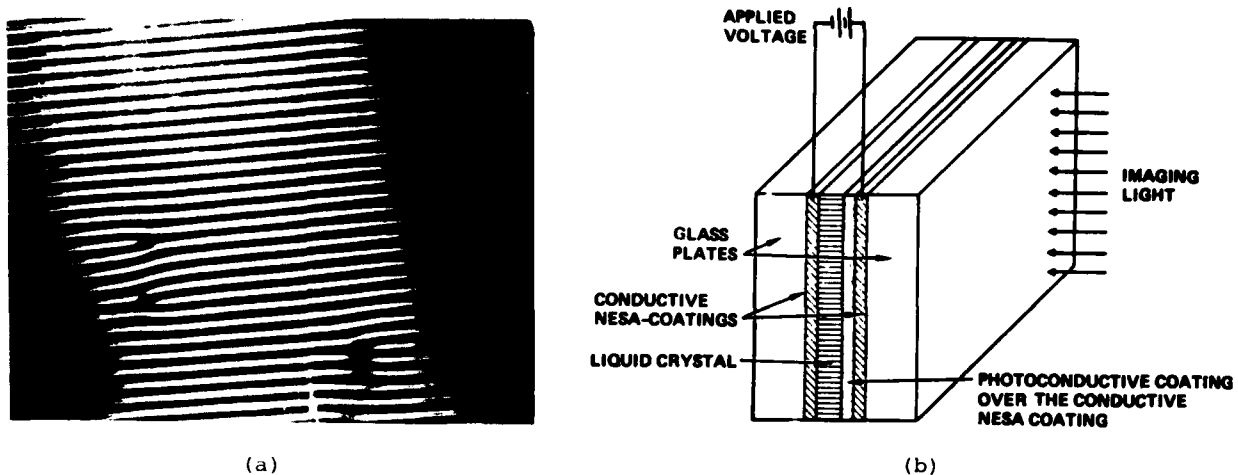


Figure 1. VGM cell. (a) The phase grating structure of the VGM device at a fixed voltage viewed through a phase contrast microscope. (b) Schematic diagram of the VGM device construction. Current devices are read out in transmission at a wavelength at which the photoconductor is insensitive.

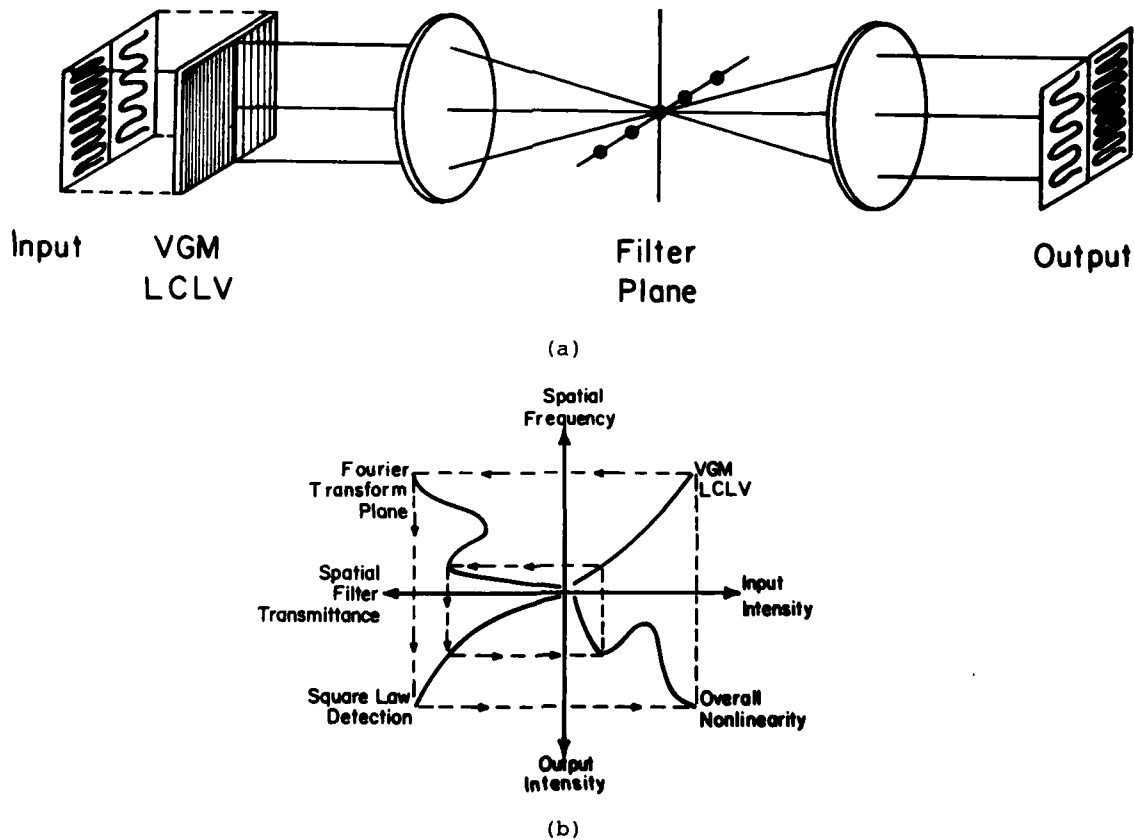


Figure 2. VGM nonlinear processing. (a) Experimental setup indicating the mapping of intensity to spatial frequency. (b) The overall input-output characteristic can be found by stepping through the successive nonlinear transformations including (1) the intensity to spatial frequency conversion, (2) spatial filtering, and (3) intensity detection.

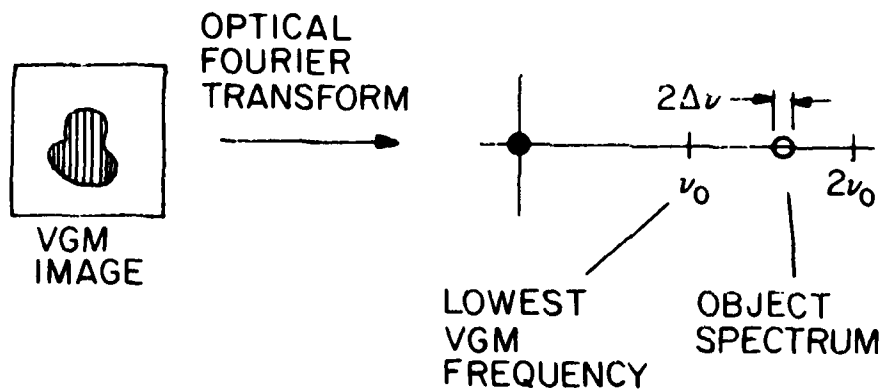


Figure 3. The gray level resolution is limited by the ratio of the distance between VGM harmonics to the object spectrum bandwidth.

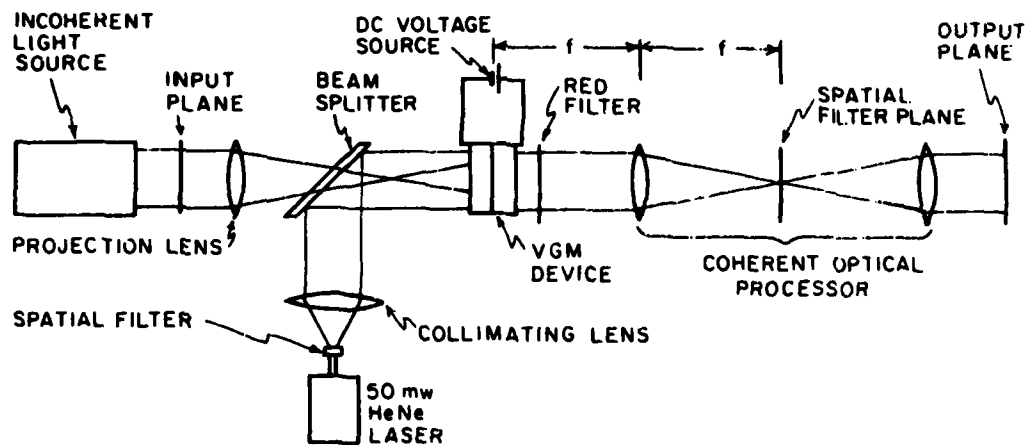


Figure 4. Experimental setup used to perform the level slice experiments. The spatial filter was a variable annular aperture.

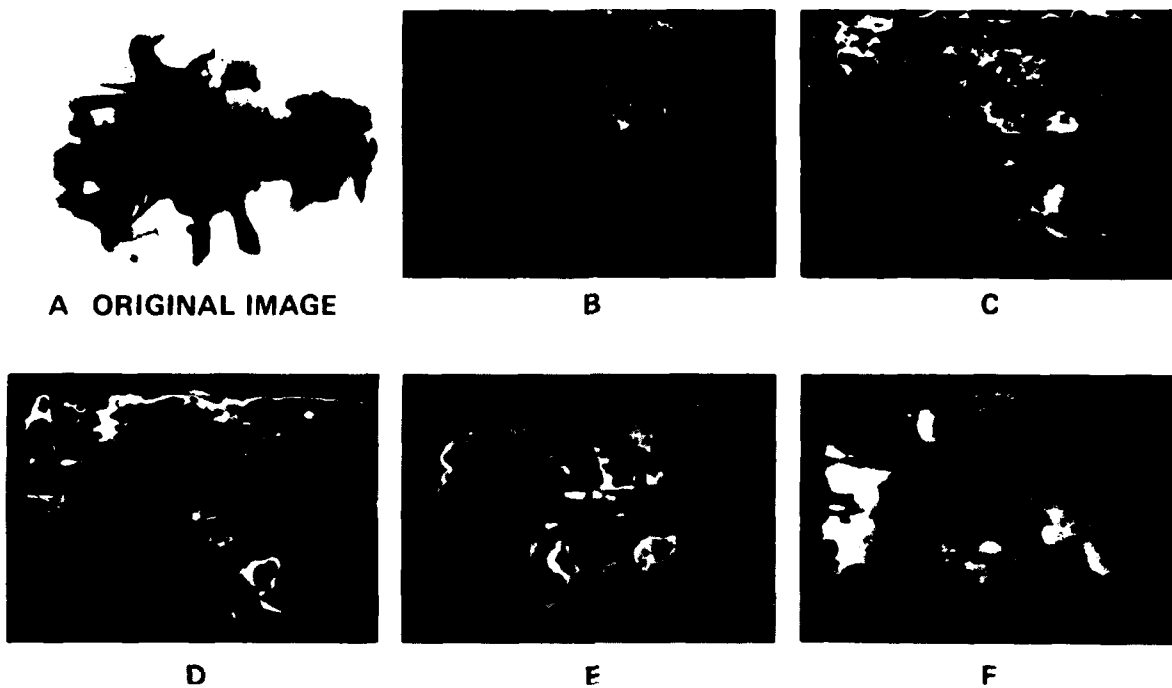


Figure 5. Level slice results. (A) Original image. (B-F) Represent level slice results for various apertures as discussed in the text.

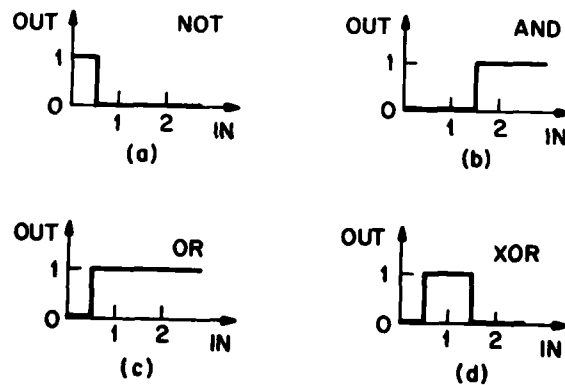


Figure 6. Logic functions as simple nonlinearities. Given an input consisting of the sum of two binary inputs, different logical operations can be effected on those inputs by means of the depicted nonlinear characteristics. (a) NOT, (b) AND, (c) OR, (d) XOR.

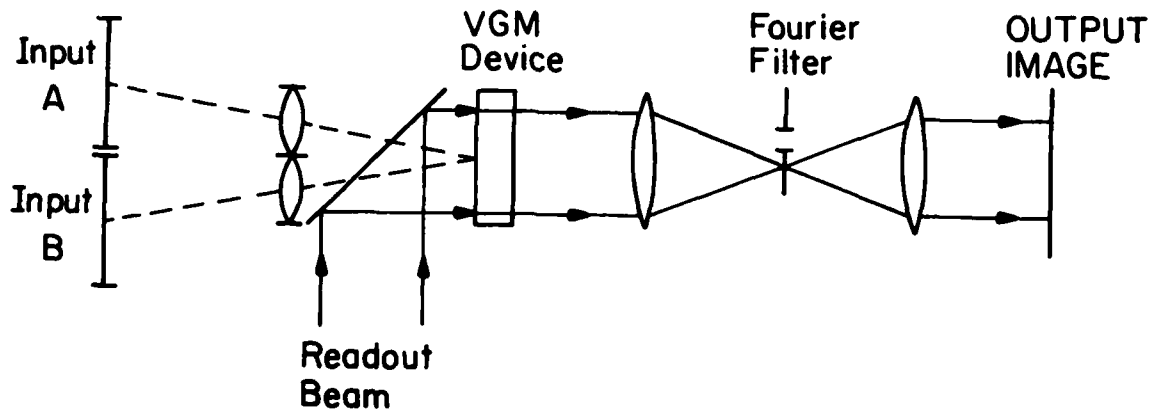


Figure 7. Experimental arrangement for performing logical operations on two dimensional binary inputs with a VGM device. The two input images are superimposed on the photoconductor. The device is read out in transmission. Simple slit apertures can be used to achieve the desired logic operations.

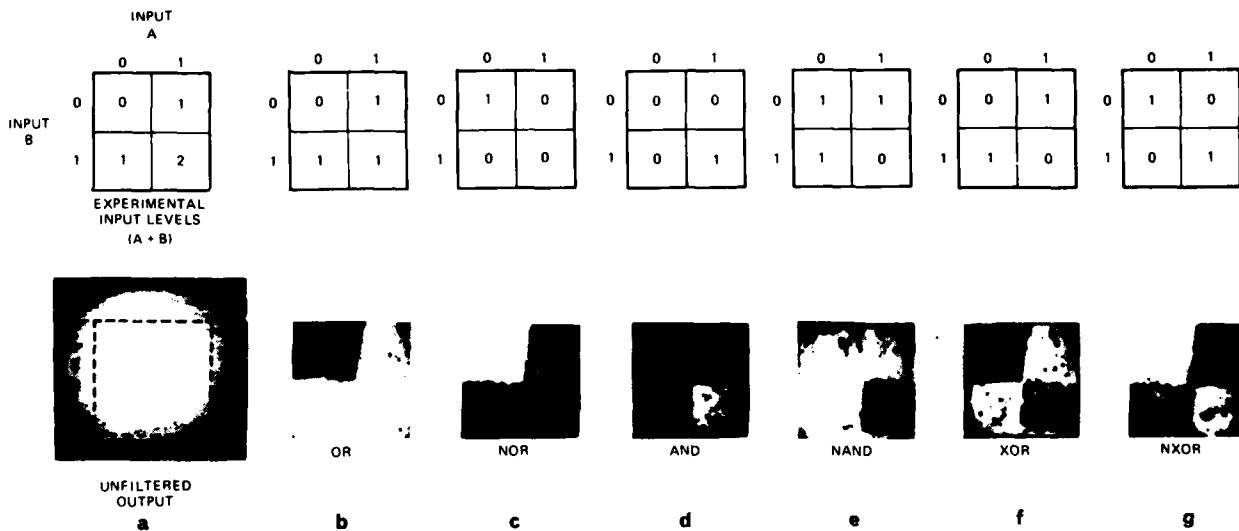


Figure 8. VGM logic results. (a) Two binary images were superimposed to produce the input intensities on the photoconductor as shown. Without any filter, the output is ideally a uniform field (logical 1). The actual output is shown below the indicated input levels. (b-g) indicate the ideal outputs and the actual outputs for the logical operations OR, NOR, AND, NAND, XOR, NXOR, respectively.

# Optical logic with variable-grating-mode liquid-crystal devices

P. Chavel,\* A. A. Sawchuk, T. C. Strand, and A. R. Tanguay, Jr.

Image Processing Institute, University of Southern California, Los Angeles, California 90007

B. H. Soffer

Hughes Research Laboratories, Malibu, California 90265

Received May 5, 1980

A liquid-crystal device that performs a two-dimensional intensity-to-spatial-frequency conversion has been investigated for use as an optical transducer. When such a device is used as the input transducer in an optical filtering arrangement, image-intensity levels can be easily manipulated by using appropriate Fourier plane filters. The variable-grating-mode liquid-crystal device is well adapted to performing binary logic operations on images. Results demonstrating the implementation of common logic operations are presented.

One of the primary concerns in optical image processing and optical computing is the desire for a wider range of real-time input transducers to meet the special requirements of various processing schemes. Variable-grating-mode (VGM) liquid-crystal devices offer a new approach to the problem of optical transducers.<sup>1,2</sup> The basic function of the VGM device is to perform an intensity-to-spatial-frequency conversion over a two-dimensional image field. In this process, the intensity variations of an input image are converted to local spatial-frequency variations in a phase-grating structure within the liquid-crystal layer. As a result of this intensity-to-spatial-frequency conversion, a standard spatial-filtering system can be used to manipulate the VGM spatial frequencies and thus the input intensities.

We describe the application of the VGM device to optical logic operations on binary images. The VGM device permits the implementation of arbitrary nonlinear point transformations of image intensity. The main advantage of the VGM approach over previous methods is the ease of programming the functional nonlinearity desired for a given image transformation. This is accomplished simply by changing the transmittance distribution of the spatial filter in the optical processor. The spatial filter is of relatively low resolution and need only have a space-bandwidth product equal to the number of gray levels to be processed independently of the space-bandwidth product of the input. This programmability advantage applies to the implementation of binary logic operations. One device can be used to implement any of the common logic operations (AND, OR, XOR, and their complements) by simply changing a Fourier plane filter. Previously described optical logic systems were "hard wired" to perform specific operations (see, for example, Refs. 3, 4, and 5). A second major advantage of the VGM system is the possibility of level restoration at each stage, which provides the requisite noise immunity. This capability has been lacking in other numerical processing systems in which noise accumulates in cascaded

stages. Considerable effort has been directed toward using integrated optics for logic elements.<sup>6-8</sup> This approach is inherently one-dimensional and does not exploit the advantages available to fully parallel two-dimensional optical processing algorithms.

The principal element of the variable-grating-mode device is a thin layer of liquid crystal that is observed to form periodic stripe domains in the presence of an applied voltage,<sup>1,2</sup> as shown in Fig. 1(a). The formation of the domains results in a phase grating characterized by a spatial frequency that depends on the magnitude of the voltage across the liquid-crystal layer. The grating period can be optically controlled by placing a

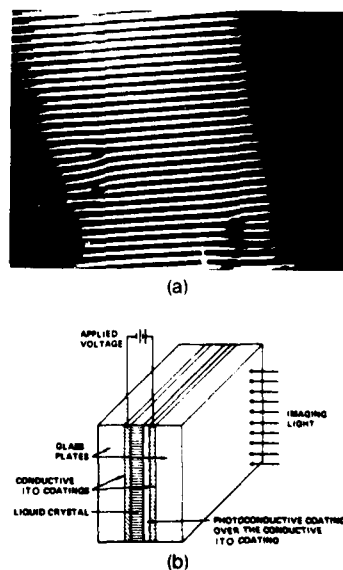


Fig. 1. VGM cell. (a) Phase structure viewed through a polarizing microscope. Typical frequencies range from 100 to 500 mm<sup>-1</sup>. (b) Schematic diagram of the VGM-device construction. At present, devices are read out in transmission at a wavelength at which the photoconductor is insensitive.

two-dimensional photoconductive layer in series with the layer of liquid crystal. The structure of the photoactivated device is shown schematically in Fig. 1(b). The sputter-deposited ZnS photoconductor and the liquid-crystal layer are sandwiched between indium-tin-oxide (ITO) transparent electrodes deposited on glass substrates. To operate the device, a dc drive voltage is impressed across the electrodes. The thin-film structure is designed to accept most of the drive voltage when the photoconductor is not illuminated, such that the fraction of the voltage that drops across the liquid crystal layer is below the activation threshold of the VGM effect. Illumination incident upon a given area of the photoconductive layer reduces its impedance, thereby increasing the voltage drop across the liquid-crystal layer and driving the liquid crystal into its activated state. Thus, because of the VGM effect, the photoconductor converts an input intensity distribution into a local variation of the phase-grating spatial frequency. The high lateral impedance of the thin photoconductive film prevents significant spreading of the photoconductivity and the associated liquid-crystal electro-optic effect. As a result, the light-activation process exhibits high resolution.

To visualize how the VGM device can be used to implement logic operations, one need only realize that the function of a logic circuit can be represented as a simple binary nonlinearity. The input-output characteristics of the common logic functions are shown in Fig. 2. The input in these figures is the simple arithmetic sum of two input image intensities corresponding to logic levels 0 or 1. For example, NOT is simply a hard-clipping inverter, AND and OR are hard-clippers with different thresholds, and XOR is a level slice function. Any spatial light modulator or optical processing system that can produce these nonlinearities can be used for implementing combinatorial logic. Furthermore, if the system allows feedback to be readily introduced, sequential or latching logic can also be implemented. The VGM device is well suited to implementing these nonlinearities. With the VGM approach, nonlinearities are obtained by using a Fourier plane filter whose transmittance variation in one dimension is essentially a plot of the desired nonlinearity. Thus arbitrary nonlinearities are easily produced and changed. Since the nonlinearities associated with logic operations are binary functions, they can be implemented with simple slit apertures, i.e., 0 or 1 transmittance values (Fig. 2). A second feature of the VGM technique that is especially suitable for logic processing is that input image and output beams are physically separate. The input beam modulates a photoconductor; concurrently the image is read out with a second beam. This separation of input and output provides for the possibility of restoring the output levels to the 0 or 1 values even if the input levels are not exactly correct. This feature is essential to the production of a reliable logic system that is immune to noise and systematic errors. Electronic logic elements possess such level-restoring capability, but previously proposed optical logic schemes lack this essential characteristic. Two further aspects of logic operations that are advantageous for optical implementation purposes are that logic operation input levels are discrete and that only a small number (2-4) of dis-

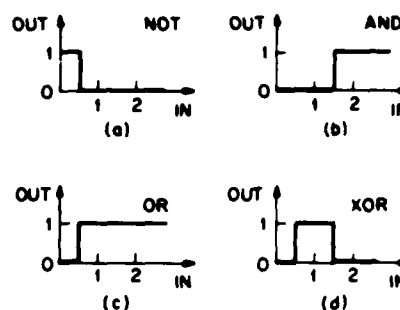


Fig. 2. Logic functions as simple nonlinearities. Given an input consisting of the sum of two binary inputs, different logical operations can be effected by means of the nonlinear characteristics depicted.

tinguishable levels are required. The existence of discrete input levels implies that the nonlinearities need not have the exact forms shown in Fig. 2. In particular, the transition regions need not be perfectly sharp thresholds since the input values are presumed not to occur within the transition regions in any event. The fact that only a few levels need be distinguished implies that the gray-level resolution requirements for the system are minimal. As an additional advantage, the input beam need not be coherent, and output coherence need only be sufficient to distinguish a small number of spatial frequencies. Many logic functions whose implementation would normally require multiple gates can be obtained directly with a single VGM cell. An important example is the full-adder, in which two input bit planes and the carry bit plane are imaged simultaneously onto the VGM device, generating four possible input intensity levels. The four resulting diffracted orders can be filtered to generate the sum bit plane by using the positive orders and simultaneously the carry bit plane by using the negative orders. Thus a full addition can be performed in a single pass through the device. Besides, functions requiring matrix-addressable look-up tables can be generated by utilizing two orthogonally oriented VGM devices in conjunction with a two-dimensional Fourier plane filter. Several such functions are required for optical implementation of residue arithmetic. Finally, in addition to the combinatorial logic functions discussed above, sequential logic may also be implemented with appropriate feedback. In this application, the output plane is imaged onto the input plane. This can be accomplished with incoherent illumination.

A series of experiments was conducted to demonstrate the fundamental logic functions. The experimental setup of Fig. 3 was used. Two input fields were superimposed at the VGM plane along with a bias illumination. The total illumination intensity on the photoconductor of the VGM device was thus the sum of the two input intensities and the bias intensity. The input illumination was a filtered high-pressure mercury-arc lamp. The bias illumination was provided by a tungsten-bulb source. The VGM device was read out in transmission, using a He-Ne laser. Filters were placed in the Fourier plane to select the diffraction orders required in each case. For these experiments, the

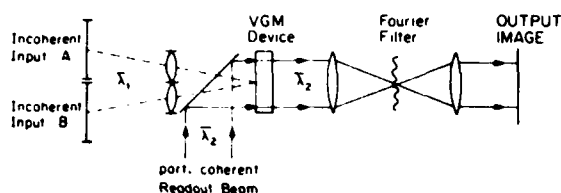


Fig. 3. Experimental arrangement for performing logical operations on two-dimensional binary inputs with a VGM device. The two input images are superimposed on the photoconductor. The device is read out in transmission. Simple slit apertures can be used to achieve the desired logic operations.  $\lambda_2$  and  $\lambda_1$  are the mean input and output wavelengths.

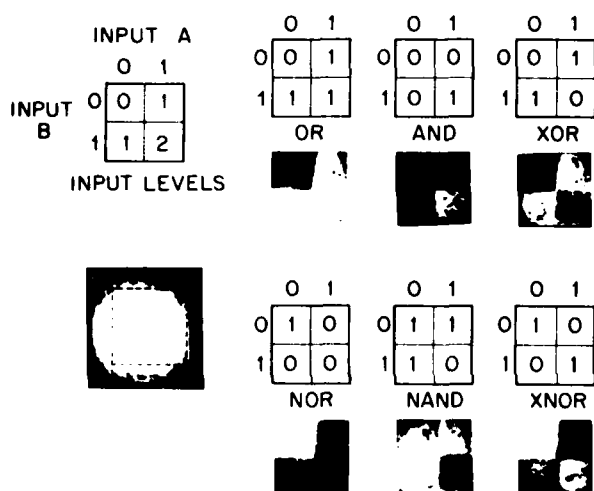


Fig. 4. VGM logic results. At left, two binary images were superimposed to produce the input intensities on the photoconductor as shown. Without any filter, the output is ideally a uniform field (logic 1). The actual output is shown below the indicated input levels. Right, ideal outputs and the actual outputs for the logical operations OR, NOR, AND, NAND, XOR, and XNOR, respectively.

inputs consisted of two rectangular apertures, one vertical and one horizontal. When these were superimposed along with the bias, a square image was formed with the four quadrants having the intensity levels shown in Fig. 4. This image corresponds to the logic truth table shown in the figure. Thus the output images have intensity levels determined by the truth table

associated with the desired logic function. The logic functions AND, OR, XOR, and their complements were implemented sequentially, as shown in Fig. 4, by altering only the Fourier plane filter. Imperfections visible in the output-plane data arise from defects in the cell structure of the VGM device employed in these experiments. Investigations of VGM-device improvements, limitations, processing speed, and pixel uniformity are in progress.

We have described the variable-grating-mode (VGM) liquid-crystal optical transducer, which operates by providing an intensity-to-spatial-frequency conversion. It has been demonstrated experimentally that this device can be used to perform combinatorial logic operations on binary images. Principal among the advantages of the VGM approach is the flexibility of the device inherent in its functional programmability, which may be exercised at will merely by changing a low-resolution spatial filter. Additional advantages include level restoration, fully parallel two-dimensional processing, and reduced coherence requirements.

The authors acknowledge the contributions of D. Boswell, A. M. Lackner, and J. D. Margerum. This research was supported by the U.S. Air Force Office of Scientific Research, Electronics and Solid State Sciences Division, under grant AFOSR-77-3285 at the University of Southern California and contract F49620-77-C-0080 at Hughes Research Laboratories.

\* Permanent address, Institut d'Optique, Université de Paris Sud, BP 43, 91406 Orsay Cedex, France.

## References

1. B. H. Soffer *et al.*, *Proc. Soc. Photo-Opt. Instrum. Eng.* **218**, 81-87 (1980).
2. P. K. Watson, J. M. Pollack, and J. B. Flannery, in *Liquid Crystals and Ordered Fluids*, J. F. Johnson and R. E. Porter, eds. (Plenum, New York, 1978), Vol. 3, pp. 421-442. See also references therein.
3. R. A. Athale and S. H. Lee, *Opt. Eng.* **18**, 513-517 (1979).
4. S. A. Collins, Jr., U. H. Gerlach, and Z. M. Zakman, *Proc. Soc. Photo-Opt. Instrum. Eng.* **185**, 36-41 (1979).
5. D. H. Schaefer and J. P. Strong III, *Proc. IEEE* **65**, 129-138 (1977).
6. L. Goldberg and S. H. Lee, *Appl. Opt.* **18**, 2045-2051 (1979).
7. S. M. Jensen, *Proc. Soc. Photo-Opt. Instrum. Eng.* **218**, 33-40 (1980).
8. E. Garmire, *Proc. Soc. Photo-Opt. Instrum. Eng.* **218**, 27-32 (1980).

SECTION 3

PERSONNEL

The professional personnel associated with the research effort at HRL  
are:

Bernard H. Soffer, Principal Investigator

Don Boswell

Anna Lackner

David Margerum

#### SECTION 4

#### REFERENCES

1. J.D. Margerum et al., Appl. Phys. Lett. 19, 216-218 (October 1971).
2. W. Grenbel and V. Wolf, Appl. Phys. Lett. 19, 213-215 (October 1971).
3. J.M. Pollack and J.B. Flannery, SID 76 Digest, pp. 143-145.
4. University of Southern California Image Processing Institute Report 720, 30 September 1976.
5. J.D. Margerum, J.E. Jensen, and A.M. Lackner, Mol. Cryst. Liq. Cryst. (in press).
6. M.I. Barnik, L.M. Blinov, A.N. Trufanov, and B.A. Umanski, J. de Physique, 39, 26 (1978).
7. A. Armand "Real Time Nonlinear Information Processing," Ph.D. Thesis, USC, EE Dept., June 1979.

## SECTION 5

### PUBLICATIONS AND PRESENTATIONS RESULTING FROM AFOSR SUPPORT

#### A. PUBLICATIONS

This section lists written publications resulting from AFOSR support from the initial starting date.

1. A. Armand, D. Boswell, A.A. Sawchuk, B.H. Soffer, and T.C. Strand, "Real-Time Nonlinear Optical Processing with Liquid Crystal Devices," Proceedings 1978 International Optical Computing Conference, London, 153-158 (September 1978).
2. A. Armand, D. Boswell, A.A. Sawchuk, B.H. Soffer, and T.C. Strand, "Approaches to Nonlinear Optical Processing in Real-Time," Proceedings International Commission for Optics Congress, Madrid, Spain, 253-256 (September 1978).
3. A. Armand, D. Boswell, J. Michaelson, A.A. Sawchuk, B.H. Soffer, and T.C. Strand, "Real-Time Nonlinear Processing with Halftone Screens," 1978 Annual Meeting, Optical Society of America, San Francisco, October 1978, Journal Optical Society of America, 68, 1361 (October 1978).
4. A. Armand, D. Boswell, A.A. Sawchuk, B.H. Soffer, and T.C. Strand, "New Methods for Real-Time Nonlinear Optical Processing," 1978 Annual Meeting, Optical Society of America, San Francisco, California, October 1978, Journal Optical Society of America, 68, 1361 (October 1978).
5. A. Armand, A.A. Sawchuk, T.C. Strand, D. Boswell, B.H. Soffer, "Real-Time Parallel Optical Analog-to-Digital Conversion," Optics Lett. 5, 129-131 (March 1980).
6. B.H. Soffer, D. Boswell, A.M. Lackner, A.R. Tanguay, Jr., T.C. Strand, and A.A. Sawchuk, "Variable Grating Mode Liquid Crystal Device for Optical Processing," Proceedings Society of Photo-Optical Instrumentation Engineers Los Angeles Technical Symposium - Devices and Systems for Optical Signal Processing, 218, 81-87, Los Angeles, California (February 1980).
7. B.H. Soffer, D. Boswell, A.M. Lackner, P. Chavel, A.A. Sawchuk, T.C. Strand, and A.R. Tanguay, Jr., "Optical Computing with Variable Grating Mode Liquid Crystal Devices," Proceedings Society of Photo-Optical Instrumentation Engineers Technical Symposium East - 1980, Optical Computing Conference, 232, 128-136, Washington, D.C. (April 1980).

8. P. Chavel, A.A. Sawchuk, T.C. Strand, A.R. Tanguay, Jr., and B.H. Soffer, "Optical Logic with Variable Grating Mode Liquid Crystal Devices," Optics Letters, Vol. 5, pp. 398-400 (September 1980).
9. B.H. Soffer, J.D. Margerum, A.M. Lackner, D. Boswell, A.A. Sawchuk, A.R. Tanguay, T.C. Strand, and P. Chavel, "Variable Grating Mode Liquid Crystal Device for Optical Processing and Computing," Molecular Crystals and Liquid Crystals, (1981).

#### B. ORAL PRESENTATIONS

This section lists oral presentations at meetings and conferences describing research supported by this contract from the initial starting date.

1. A. Armand, D. Boswell, A.A. Sawchuk, B.H. Soffer and T.C. Strand, "Approaches to Nonlinear Optical Processing with Liquid Crystal Devices," presented at the 1978 International Optical Computing Conference, London (September 1978).
2. A. Armand, D. Boswell, A.A. Sawchuk, B.H. Soffer, and T.C. Strand, "Approaches to Nonlinear Optical Processing in Real-Time," presented at the International Commission for Optics Congress, Madrid, Spain (September 1978).
3. A. Armand, D. Boswell, J. Michaelson, A.A. Sawchuk, B.H. Soffer, and T.C. Strand, "Real-Time Nonlinear Processing with Halftone Screens," presented at 1978 Annual Meeting, Optical Society of America, San Francisco, California (October 1978).
4. A. Armand, D. Boswell, A.A. Sawchuk, B.H. Soffer and T.C. Strand, "New Methods for Real-Time Nonlinear Processing," presented at 1978 Annual Meeting, Optical Society of America, San Francisco, California (October 1978).
5. A.A. Sawchuk, T.C. Strand, A.R. Tanguay, Jr., P. Chavel, D. Boswell, and B.H. Soffer, "Parallel Optical Analog-to-Digital Conversion Using a Liquid Crystal Light Valve," Workshop on High Speed A/D Conversion, Portland, Oregon (February 1980).
6. B.H. Soffer, D. Boswell, A.M. Lackner, A.R. Tanguay, Jr., T.C. Strand, and A.A. Sawchuk, "Variable Grating Mode Liquid Crystal Device for Optical Processing," presented at SPIE Los Angeles Technical Symposium-Devices and Systems for Optical Processing, Los Angeles, California (February 1980).

7. B.H. Soffer, D. Boswell, A.M. Lackner, P. Chavel, A.A. Sawchuk, T.C. Strand, and A.R. Tanguay, Jr., "Optical Computing with Variable Grating Mode Liquid Crystal Devices," SPIE Technical Symposium East-1980 Optical Computing Conference, Washington, D.C. (April 1980).
8. A.A. Sawchuk, T.C. Strand, A.R. Tanguay, Jr., P. Chavel, D. Boswell, A.M. Lackner and B.H. Soffer, "Variable Grating Model Liquid Crystal Light Valves and their Application to Optical Processing," Gordon Research Conference on Coherent Optics and Holography, Santa Barbara, California (June 1980).
9. B.H. Soffer, D. Boswell, A.M. Lackner, A.R. Tanguay, Jr., T.C. Strand, and A.A. Sawchuk, "Variable Grating Mode Liquid Crystal Devices for Optical Processing and Computing," Eighth International Liquid Crystal Conf., Kyoto, Japan (June 1980).

